Lancaster Environment Centre

LEC Technical Report 2019

Hypothetico-Inductive DBM modelling of Globally Averaged Surface Temperature

Peter C. Young

Abstract

This report considers an inductive, *Data-Based Mechanistic* (DBM) approach to modelling the dynamic relationship, in the form of an ordinary differential equation model, between global averaged measures of total radiative forcing and atmospheric temperature, in which the model structure is inferred from the data. In contrast to previous research (Young, 2014, 2018), this report concentrates on the estimation of important, climatically meaningful parameters, such as the 'Climate Sensitivity'; 'Feedback Response Time' (time constant); and 'Effective Heat Capacity' that can be derived from the DBM model. It also considers the nature of the model response, which includes an oscillatory component with a period of about 50 years; and how the model can be used in applications such as scenario and hypothetical forecasting.

1 Introduction

A previous report (Young, 2014)[1] and associated paper (Young, 2018) have shown that low dynamic order models are able to emulate the behaviour of large climate simulation models. Moreover, when such low order models are

[1]This report can be downloaded from `http://captaintoolbox.co.uk/Captain_Toolbox.html/Publication_Downloads.html` as `HIDBM_Climate1.pdf`, but note that some of the analysis therein has been superseded by that presented here.

inferred directly from global climate data, using the *Data-Based Mechanistic* (DBM) approach to the inductive modelling of dynamic systems (see e.g. Young, 2011, 2012, and the prior references therein), they produce reasonable short-to-medium forecasts of global temperature, including a prediction of the 'levelling' in temperatures that occurred after the start of the new Millennium.

Defining the objectives of a model-based study is the first step in the DBM approach to modelling and this previous research was aimed mainly at the forecasting of globally averaged surface temperature. The objectives of the present report are somewhat different. They are to synthesize a constant parameter, continuous-time differential equation DBM model from which important, climatically meaningful parameters can be derived. This has to be a stochastic model, obtained using optimal methods of statistical inference, because it is important to not only estimate the parameters but also to quantify the uncertainty in these estimates.

Such differential equation models have a number of advantages, from both scientific and statistical standpoints (Garnier and Young, 2014). In the context of climate system modelling, for instance, differential equation models are of the same general form as those used in the construction of global climate models, albeit very much smaller, with a lower dynamic order that captures the identifiable 'dominant modes' of the global system; and they are characterized by parameters that have immediate physical meaning and appropriate units that quantify this meaning.

Most importantly, DBM models are not the kind of 'black-box' time series/econometric models that have been used previously to model globally averaged data (see for example Kaufmann et al., 2006; Mills, 2009). They are models that can be interpreted directly in physically meaningful terms that adds to their credibility in scientific terms. In the present context, for example, they allow for the simple derivation of parameters, such as the 'Climate Sensitivity'; 'Feedback Response Time' or 'Time Constant'; and 'Effective Heat Capacity' that have a important and well defined climatic meaning. As we shall see, the models are also in an ideal form for applications such as scenario analysis, hypothetical forecasting and emissions management.

2 Global Average Temperature

DBM modelling involves several stages that have been described fully in previous publications (see e.g. Young and Ratto (2009); Young (2016), as well as chapter 12 in Young, 2011, and the prior references therein). In the present context it involves the identification of the continuous-time *Transfer Function* (hereafter denoted by TF) model structure from the available globally averaged data, followed by the optimal estimation of the parameters that characterize this TF model. These estimated parameters are associated directly with the identified TF model or, equivalently, the differential equations defined by this TF which, in the present context, are a better known form of the dynamic equations within the climate community. In fact, the final form of the DBM model is estimated by nonlinear optimization using 'prediction error minimization' based on a Simulink^{TM}representation of these differential equations.

The *climatically meaningful* parameters that chracterize the optimized model are derived from the estimated parameters of the differential equation model. Consequently, the uncertainty in these derived parameters is evaluated using *Monte Carlo Simulation* (MCS) analysis based on the estimated uncertainty in the directly estimated parameters (as defined by their estimated error covariance matrix). This MCS analysis also allows for the quantification of the uncertainty associated with the response of the DBM model to the TRF input.

2.1 The Globally Averaged Climate Data

The data used for statistical model identification and estimation in this report are the annual, globally averaged climate data, as plotted in figure 1 for the historical period from 1856 to 2015[2]. These data are derived from the global averaging of measurements, carried out by climate scientists, and it is assumed here that this global averaging is a legitimate statistical procedure for inferring the changes in the variables at the global level. The *Globally Averaged Temperature Anomaly* (GTA) shown in the

[2]Data download sites: `http://cdiac.ornl.gov/trends/temp/jonescru/jones.html`; `http://www.pik-potsdam.de/~mmalte/rcps/`; `http://www.cgd.ucar.edu/cas/catalog/climind/AMO.html`. Note: The data from these sites were accessed in 2009, when the present study was initiated, and they can change, so the GTA, RTF and AMO data sets used in the present paper can be downloaded as Climate Data.zip from `http://captaintoolbox.co.uk/Captain_Toolbox.html/Publication_Downloads.html`

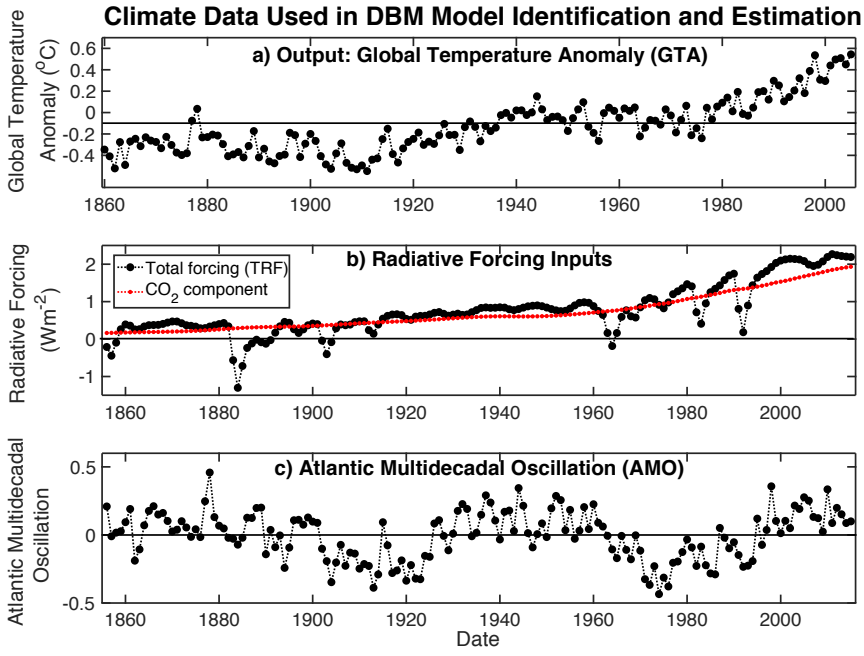

Figure 1: **Globally averaged climate data**. Top panel: GTA measurements, from the Carbon Dioxide Information Analysis Center (CDIAC). Middle panel: the RTF signal and the CO_2 component of this total signal, from the Potsdam Institute for Climate Impact Research website. Lower panel: the AMO series, downloaded from the Physical Sciences Division, Earth System Research Laboratory of NOAA.

upper panel of figure 1 represents the changes in the globally averaged surface temperature around a level defined by the background average of the temperature measurements over the period 1950 to 1980. The panel below this shows the changes in the *Total Radiative Forcing* (TRF). The Intergovernmental Panel on Climate Change (IPCC) AR4 report (see `https://www.ipcc.ch/pdf/assessment-report/ar4/syr/ar4_syr.pdf`) defines radiative forcing as follows:

"Radiative forcing is a measure of the influence a factor has in altering the balance of incoming and outgoing energy in the Earth-atmosphere system and is an index of the importance of the factor as a potential climate change mechanism. The radiative forcing values are for changes relative to preindustrial conditions defined at 1750 and are expressed in Watts per square meter (W/m^2)"

The TRF, shown by the black line, is made up of several components. The important CO_2 component is shown as the red dotted line; and the sharp negative excursions in the TRF are associated with volcanic eruptions.

The lower panel in figure 1 shows the *Atlantic Multidecadel Oscillation* (AMO) which was identified by Schlesinger and Ramankutty (1994). The AMO signal is usually defined from the patterns of SST variability in the North Atlantic once a trend has been removed. For instance, the Schlesinger and Ramankutty trend removal is based on the global-mean temperature changes simulated by a simple, hemispherically resolved, climate/ocean model: i.e., the simulated changes are subtracted from the observed global-mean temperature changes to reveal what, it is assumed, is not caused by radiative forcing. When modelling systems that include trend behaviour such as this, detrending is not recommended unless there is no other way of explaining the presence of the trend. This is because detrending is not a particularly well-defined operation and may remove dynamic artefacts that are important in the dynamic modelling[3]. Consequently it would be preferable to use the original data without any trend removal but we do not have access to these data.

All of the data are affected by uncertainty that arises from various causes, as discussed briefly at the beginning of the IPCC report. In the present report, it is assumed that this uncertainty results in unexplained additive noise on the TF model that is modelled by a discrete-time AutoRegressive (AR) model. In other words, the full DBM model is a 'hybrid' combination of the continuous-time differential equation model relating the total radiative forcing to the GTA and AMO and a discrete-time, difference equation, noise model. Such a hybrid model avoids certain difficulties associated with the estimation of continuous-time noise models (see Appendix B, section B.3.5 in Young, 2011) and (page 156 et seq., in Priestley, 1988). The presence of the additive noise, which accounts for about 10% of the variance in the GTA data, is reflected in the uncertainty on the estimates of the TF model parameters, as quantified by the optimization procedures used for model estimation.

[3]This is discussed later in section 3.1, where an alternative approach is utilized that does not suffer from these disadvantages.

2.2 Global Climate Parameters

The most important parameters of any model used to explain the changes in the globally averaged data in figure 1 are concerned with the transient and equilibrium behaviour of the model at this globally averaged level. For instance, if the model is stable and is perturbed by a constant radiative forcing input, what globally averaged temperature does it reach at equilibrium and what time does it take to reach this equilibrium level?

The best known parameter of this kind is the *Global Equilibrium Climate Sensitivity*, which will be denoted here by ECS. ECS has a component directly due to radiative forcing by CO_2, and a further contribution arising from any positive or negative feedback effects within the climate system. Without any such effects, climate scientists claim that a doubling of CO_2, which is equivalent to an increase in forcing of $3.7W/m^2$, would result in a one degree centigrade increase in the global temperature. However, there are likely to be feedback effects in the global system that will change this value and should be reflected also in the measured changes shown in figure 1. The most important DBM model parameter that affects the equilibrium is the *Steady State Gain* (G), i.e. if the equilibrium level of the globally averaged temperature, $x(t)$, is denoted by $x(\infty)$, and the steady level of the radiative forcing is denoted by $u(\infty)$, then $x(\infty) = Gu(\infty)$.

In reaching its equilibrium level, any stable dynamic system will undergo transient dynamic behaviour, the importance of which in the case of possible global warming is obvious. The model parameters that affect this transient behaviour are the *Time Constant* (T) of any first order dominant mode; and, if the response of the system is oscillatory, the *Natural Frequency* (ω_n), the natural period of this oscillation ($P_n = 2\pi/\omega_n$) and the associated *Damping Ratio* (ζ) (see Appendix B in Young, 2011).

3 DBM Model Identification and Estimation

The general, DBM model used in this paper is a linear, multi-input, continuous-time TF model that can be written informally[4] as follows:

$$\begin{aligned} \text{Deterministic Model}: \quad & x(t) = \sum_{i=1}^{nu} \frac{B_i(s)}{A_i(s)} u_i(t-\tau_i) \\ \text{Noise Model}: \quad & \xi(k) = \frac{D(z^{-1})}{C(z^{-1})} e(k); \qquad e(k) = \mathcal{N}(0, \sigma^2) \\ \text{Observation Equation}: \quad & y(k) = x(k) + \xi(k) \end{aligned} \tag{1}$$

where τ_i represents a pure time delay between the input variable $u_i(t)$ and its first effect on the output $x(t)$; s is differentiation operator, i.e. $s^r = d^r/dt^r$, so that $s^r x(t) = \frac{d^r x(t)}{dt^r}$; and $A_i(s)$, $B_i(s)$ are appropriately defined polynomials in s of the following form:

$$\begin{aligned} B_i(s) &= b_{0i} s^{m_i} + b_{1i} s^{m_i - 1} + \ \ldots, + b_{m_i i} \\ A_i(s) &= s^{n_i} + a_{1i} s^{n_i - 1} + a_{2i} s^{n_i - 1} + \ \ldots, + a_{n_i i} \end{aligned} \tag{2}$$

The discrete-time noise model is, in general, an *AutoRegressive Moving Average* (ARMA) process defined by the polynomials $C(z^{-1})$ and $D(z^{-1})$ of the following form:

$$\begin{aligned} C(z^{-1}) &= 1 + c_1 z^{-1} + c_2 z^{-2} + \ \ldots \ + c_p z^{-p} \\ D(z^{-1}) &= 1 + d_1 z^{-1} + d_2 z^{-2} + \ \ldots \ + d_q z^{-q} \end{aligned} \tag{3}$$

where z^{-r} is the backward shift operator, i.e. $z^{-r}\xi(k) = \xi(k-r)$. A multi-output system can be defined as an amalgamation of single output models such as this.

The total model structure is specified by the vector

$$[n_i \ m_i \ (i = 1, 2, \ \ldots, nu) \ \tau_i \ (i = 1, 2, \ \ldots \ nu) \ p \ q]$$

Identification of the model structural parameters in this vector, as well as the estimation of the polynomial parameters ($a_{i,j}$, $i = 1, 2, \ \ldots, n$; $j = 1, 2, \ \ldots, nu$, $b_{i,j}$, $i = 1, 2, \ \ldots, m$; $j = 1, 2, \ \ldots, nu$, c_i, $i = 1, 2, \ \ldots, p$, d_i, $i = 1, 2, \ \ldots, q$ and σ^2) that characterize the associated model, is a well known

[4] Informal because its involves a mixture of the two operators s and z^{-1}.

statistical problem of time series analysis. In DBM modelling, it is normally solved by maximum likelihood estimation using the *Refined Instrumental Variable* method (see e.g. Young, 2011, 2015) for hybrid continuous-time models of this type (RIVC). This is available as the rivcbjid and rivcbj routines in the CAPTAIN Toolbox[5] for Matlab^{TM}, which is used in most of the DBM modelling exercises considered in subsequent sections of this report.

The continuous-time TF model (1) is simply a concise and convenient way of representing the better known differential equation models used in most climate research. One advantage of this model form is that it can be related directly with the Laplace transform transfer function form of differential equation models. Indeed, s is often used as the Laplace operator and it is used here as the derivative operator to emphasize this relationship. If there are no initial conditions affecting the data, then the Laplace transform and derivative operator forms of the TF are identical. If there are initial conditions effects present, however, the Laplace transform of the differential equation introduces additional terms that are dependent on the initial conditions of the output, input and their time derivatives. This is discussed in Appendix A, which shows how accounting for the initial conditions is not difficult and can be used to good effect in the model estimation. As we shall see, in the present study, it can avoid the need to detrend the GTA series prior to time series modelling, a questionable device often employed by time series analysts.

In order to examine this relationship between continuous-time TF and differential equation models in simple terms, let us consider a first order, two-input model of the above type, as identified in the next sub-section 3.1. This takes the following form, which has the structure vector [1 2 2 0 0 1 0]:

$$\begin{aligned} x(t) &= \frac{b_{01}s + b_{11}}{s + a_{11}}u(t) + \frac{b_{02}s + b_{12}}{s + a_{11}}u_{IC} \\ \xi(k) &= \frac{1}{1 + c_1 z^{-1}}e(k); \qquad e(k) = \mathcal{N}(0, \sigma^2) \\ y(k) &= x(k) + \xi(k) \end{aligned} \tag{4}$$

Here u_{IC} is a second, artificial input, set to unity over the whole observational interval, which simply allows for the estimation of the initial conditions and their effects on the output response $x(t)$, as discussed in Appendix A.

[5]The CAPTAIN Toolbox is freely available via the website `http://captaintoolbox.co.uk/Captain_Toolbox.html/Captain_Toolbox.html`

However, the main description of the system dynamics resides in the first transfer function between $u(t)$ and $x(t)$. In the present context, $u(t)$ is the measured TRF input and $x(t)$ is the deterministic output of the model, i.e. the model's estimate of that part of the measured GTA response that is not contaminated by the 'noise' $\xi(k)$, which could represent random measurement noise but might account for other, unexplained perturbations in the measured response not explained by the model.

The deterministic part of the model (4) between $u(t)$ and $x(t)$ is directly equivalent to the following, first order differential equation:

$$\frac{dx(t)}{dt} + a_{11}x(t) = b_{01}\frac{du(t)}{dt} + b_{11}u(t) \tag{5}$$

which is obtained by simply multiplying throughout the equation by $s + a_{11}$ and applying the s operator wherever this appears (here in relation to $x(t)$ and $u(t)$, yielding $\frac{dx(t)}{dt}$ and $\frac{du(t)}{dt}$). One advantage of continuous-time models such as this is that the dynamic nature of the system can be inferred immediately from the parameters in the model, without having to resort to the solution of the underlying differential equation. For example, the dynamic nature of this first order model is defined completely by the following two 'derived' parameters:

$$\begin{aligned} \text{Steady State Gain} \quad G &= \frac{b_{11}}{a_{11}} \\ \text{Time Constant} \quad T &= \frac{1}{a_{11}} \end{aligned} \tag{6}$$

As we shall see, both of these parameters have important implications in the present climate context, where G is directly proportional to the ECS that defines the equilibrium level of the globally averaged temperature; and T that defines the time taken for the system to reach $1 - e^{-1} = 0.632$ of the final equilibrium level[6].

A second order example of the TF model (1), as identified later in subsection 3.2.1, has a structure vector [2 2 2 0 0 1 0] and the main TF between $u(t)$ and $x(t)$ takes the form:

$$x(t) = \frac{b_{01}s + b_{11}}{s^2 + a_{11}s + a_{12}}u(t - \tau) \tag{7}$$

[6]This has been termed 'Feedback Response Time' in climate publications: see section 3.7.1

which defines a differential equation model of the form:

$$\frac{d^2x(t)}{dt^2} + a_{11}\frac{dx(t)}{dt} + a_{12}x(t) = b_{01}\frac{du(t-\tau)}{dt} + b_{11}u(t-\tau) \tag{8}$$

Once again, physically meaningful parameters derived from the parameters in this equation immediately provide details of the system transient response. In this case, these are:

$$\begin{aligned} \text{Steady State Gain} \quad G &= \frac{b_{11}}{a_{12}} \\ \text{Natural Frequency} \quad \omega_n &= \sqrt{a_{12}} \text{ radians/time unit} \\ \text{Natural Period} \quad P_n &= \frac{2\pi}{\omega_n} \text{ time units} \\ \text{Damping Ratio} \quad \zeta &= \frac{a_{11}}{2\omega_n} = \frac{a_{11}}{2\sqrt{a_{12}}} \end{aligned} \tag{9}$$

If the damping ratio ζ is less than its 'critically damped' value of unity, then the transient response will exhibit oscillatory behaviour at a frequency defined by the natural frequency ω_n with an associated natural period P_n. If $\zeta = 0$, then the oscillations are undamped and the oscillatory response is sustained; whereas for $0 < \zeta < 1.0$ they are damped in time and die out unless the system is perturbed by a change in the input $u(t)$.

These derived parameters also have relevance in a climate context. We will see that a model of the form (8), with $b_{11} = 0$, is identified, in section 3.2.1, for the behaviour of an oscillatory component, denoted by $x_2(t)$, in a model between the TRF and the GTA, where ω_n defines the oscillatory frequency of the series, and an associated small value for ζ shows that the oscillations are almost undamped. Another model of this form, but with b_{11} present, is identified, in section 3.5, for the relationship between $x_2(t)$ and the AMO series.

In cases where the damping ratio is ≥ 1.0, it sometimes assist in the physical interpretation of the model, to decompose the second order equation (8) into a serial or feedback connection of two first order TFs, the time constants of which are based on the real roots of the factorized TF denominator $s^2 + a_{11}s + a_{12} = (s + \alpha_1)(s + \alpha_2)$, where $-\alpha_1 = -1/T_1$ and $-\alpha_2 = -1/T_2$ are the 'eigenvalues' of the model. Examples of such feedback decomposition are discussed later in sections 3.7.2 and 3.7.3.

3.1 Initial Model Structure Identification

In this report, the objective of the DBM modelling is to identify and estimate a continuous-time TF model, based on the data shown in figure 1, that explains as much of the variation in GTA and AMO series as possible, under the assumption that this variation is primarily the result of the changes in the radiative forcing inputs. The GTA and TRF data are both characterized by a rising trend and the presence of such a trend is often considered in the time series literature (e.g. Box and Jenkins, 1970; Box et al., 1994) as 'nonstationarity' in the data, the effect of which should be removed prior to modelling using either some form of differencing to render the series stationary, or alternatively some form of 'detrending' (see earlier comments in section 2.1).

Neither of these standard statistical approaches seem very satisfactory in this case because the trend in the GTA can be explained by the trend in the TRF input and the trend in the RTF is arising because of assumed known factors associated with natural and anthropogenic activity. Moreover, the analysis in subsequent sections will show that the relationship between the TRF and GTA, which is the primary object of the present study, can be identified satisfactorily if the initial conditions on the data are estimated and, as discussed previously, accounted for in the model estimation.

Another important aspect of the data shown in figure 1 is that they derive from the measured behaviour of the global system during its 'normal functioning'. In other words, we have to accept the data in this limited form, with no possibility of performing the planned experiments that are so important in Popper's hypothetico-deductive approach. In the systems and control literature, it is assumed that the inputs to a dynamic system are 'sufficiently exciting' to allow for satisfactory identification and estimation of the input-output model (see e.g. Young, 2011). Consequently, we have to assume, in the first instance, that the radiative forcing inputs are sufficiently exciting in this sense. Except for the effects of volcanic activity, however, the natural variations in the TRF data are not particularly pronounced, so this must be be taken into account when evaluating the efficacy of the finally estimated model.

With the above observations and caveats in mind, an obvious first step in the modelling is to consider the identification and estimation of a simple model between TRF and GTA, which should include the estimation of initial conditions on the data, as well as the effects of these initial conditions on

the subsequent dynamic behaviour. The simplest initial approach to such model identification and identification is to use the rivcbjid model structure identification routine in the CAPTAIN Toolbox. For simplicity, this assumes a common denominator $A(s)$ in the TF model (i.e. $A_i(s) = A(s) \forall i$) and it yields the table below (verbatim, as produced by rivcbjid).

```
------------------- BEST 10 models (Rt2) --------------------
den num del AR  MA    YIC       RT2         BIC          AIC
 3   4   0   2   0  -1.3879   0.900151   -714.4758   -4.7403
     4   0
 3   3   0   2   0  1.5802    0.882592   -698.7534   -4.6228
     4   0
 2   2   0   2   0  -0.2943   0.879561   -712.0321   -4.6482
     3   0
 3   4   0   2   0  -1.2335   0.876765   -691.8634   -4.5798
     3   0
 3   3   0   2   0  -1.0084   0.875575   -694.4475   -4.5767
     3   0
 3   2   0   2   0  1.4406    0.863789   -663.7441   -4.3656
     3   0
 3   2   0   2   0  10.5985   0.861089   -646.7842   -4.2404
     2   0
 3   2   0   2   0  -0.0510   0.846470   -656.2989   -4.3383
     4   0
 3   3   0   2   0  8.4910    0.668903   -157.7879   -1.2034
     2   0
 2   3   0   2   0  2.0582    0.546351   -659.6170   -4.3398
     3   0
```

In this table, the two rows in the numerator ('num') and time delay ('del') columns, for each model, relate to the two inputs $u(t)$ and u_{IC} in the model (4). 'YIC', 'BIC' and 'AIC' are logarithmically defined identification criteria (see chapter 6 of Young, 2011, for their definitions and explanation of how they are used) where the lowest, normally most negative, value indicates those models that provide the best compromise between the explanation of the data and the number of parameters required to achieve this. Finally, 'RT2' is the *Coefficient of Determination* R_T^2 based on the error $e(k) = y(k) - \hat{x}(k)$ between the simulated model output $\hat{x}(k)$ and the measured GTA $y(k)$, i.e.,

$$R_T^2 = 1 - \frac{\sigma^2}{\sigma_y^2}; \tag{10}$$

where σ^2 is the variance of $e(k)$ and σ_y^2 is the variance of $y(k)$, both about their mean values. Consequently, the closer the value of R_T^2 to unity, the better the explanation $y(k)$.

The table shows that the 3rd order model with structure [3 4 4 0 0 2 0] not only provides the best explanation of the data, with $R_T^2 = 0.90$, but is also selected by all the model identification criteria YIC, BIC and AIC. This hybrid model is presented below in a decomposed form with the output of the main TF in (i) denoted by the state $x_1(t)$; the output of the initial condition TF in (ii) denoted by the state $x_i(t)$; the observation equation (iii) showing the sampled output as the sum of the two sampled states; and the noise $\xi(k)$, which is identified as a second order AR(2) model in (iv).

$$\begin{aligned}
x_1(t) &= \frac{b_{01}s^3 + b_{11}s^2 + b_{21}s + b_{31}}{s^3 + a_{11}s^2 + a_{21}s + a_{31}}u(t) && (i)\\
x_i(t) &= \frac{b_{02}s^3 + b_{12}s^2 + b_{22}s + b_{32}}{s^3 + a_{11}s^2 + a_{21}s + a_{31}}u_{IC} && (ii)\\
\xi(k) &= \frac{1}{1 + c_1z^{-1} + c_2z^{-2}} + e(k) \qquad e(k) = \mathcal{N}(0, \sigma^2) && (iii)\\
y(k) &= x_1(k) + x_2(k) + \xi(k) && (iv)
\end{aligned} \tag{11}$$

The estimates of the parameters are as follows, with the standard errors shown in parentheses:

$$\begin{aligned}
&\hat{a}_{11} = 0.0483(0.026);\ \hat{a}_{21} = 0.0126(0.0018);\ \hat{a}_{31} = 0.000586(0.00028)\\
&\hat{b}_{01} = 0.0719(0.028);\ \hat{b}_{11} = 0.0294(0.012);\ \hat{b}_{21} = 0.000963(0.000988)\\
&\hat{b}_{31} = 0.000368(0.000144);\ \hat{b}_{02} = -0.370(0.049);\ \hat{b}_{12} = 0.0267(0.0172)\\
&\hat{b}_{22} = -0.00391(0.000593);\ \hat{b}_{32} = -0.000279(0.000131)\\
&\hat{c}_1 = -0.259(0.079);\ \hat{c}_2 = 0.200(0.079);\ \hat{\sigma}^2 = 0.0076
\end{aligned} \tag{12}$$

As would be expected from the $R_T^2 = 0.90$, the model (11) explains the data quite well, as shown in the upper panel of figure 2; and, as required, the model residual series $e(k)$ is both serially uncorrelated and uncorrelated with the TRF input series, showing that it is playing no statistically significant part in explaining the relationship between $u(t)$ and $x(t)$. However, (12) is a quite high order model with a total of 14 parameters in the continuous-time model and 2 in the AR(2) noise model. The component responses from the

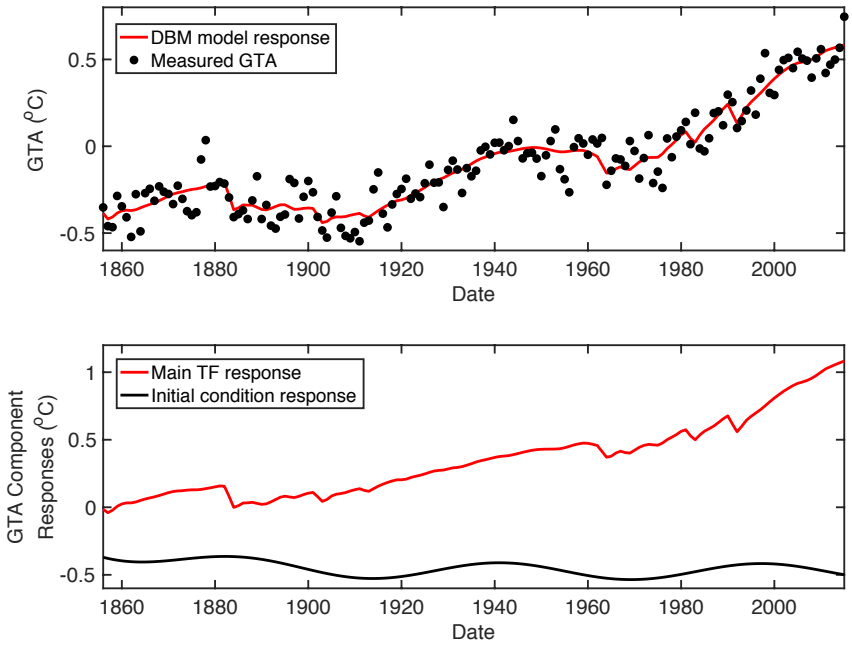

Figure 2: The upper panel compares the output of the initial model with the GTA data and the components of this response are shown in the lower panel.

two TFs plotted in the lower panel of figure 2 are quite revealing. They show that the initial condition response is dominated by a very low damped sinusoidal signal which accounts for low level cyclic behaviour which we can now see is appearing in the GTA response.

The nature of this oscillatory component can be ascertained from the 3 roots (poles) of the 3rd order TF denominator. One of these is a real root with a value -0.0466, which defines a first order response with a time constant $T_2 = 1/0.0466 = 21.5$ years. The others are a complex conjugate pair at $-0.000842 \pm 0.112i$ that are associated with a second order polynomial of the form $s^2 + 2\zeta\omega_n s + \omega_n^2$ that defines the natural frequency as $\omega_n = 0.112$ radians/second with an associated, very small, damping ratio of $\zeta = 0.0075$. Consequently, the period of the oscillation is $2\pi/0.112 = 56.1$ years which can be linked with the period of the quasi-cyclic component identified in Young (2018); and is also somewhat similar to the quasi-cyclic period of 62.5 years (see later section 3.7.3) that is evident in the AMO series shown in figure 1.

As we are concerned with climate parameters in this paper, it is interesting to note that, although this is the first, simple step in the modelling

exercise, the initial model (11) can provide estimates $\hat{\text{ECS}}$, $\hat{T}$ and $\hat{P}_n$ of the globally averaged climate parameters (see earlier section 2.2). And since it is a stochastic model, we are able to compute the uncertainty in these estimates, based on the directly estimated model parameters in (12) and their associated covariance matrix, using *Monte Carlo Simulation* (MCS) analysis (see also later section 3.3). The estimates obtained in this manner, using MCS analysis based on 10,000 random realizations, are shown in Table 1 with plots of the frequency distribution of $\hat{\text{ECS}}$ and the associated response of the model to a step of 3.7 W/m^2, equivalent to a doubling of atmospheric CO_2, in figure 3. The very small oscillations in this step response derive from the oscillatory mode discussed above. However, most of this oscillatory mode is connected with the intial condition response which, as we shall see later, is accounting for a disproportionate proportion of this oscillatory behaviour.

Parameter	Estimate	Lower 5% Bound	Upper 95% Bound
$\hat{CS}$ (^{o}C)	2.32	2.05	3.34
$\hat{T}$ (years)	21.4	13.2	72.6
$\hat{P}_n$ (years)	56.1	51.8	63.2

Table 1: MCS results for the Initial DBM Model based on $10,000$ random realizations defined by the estimated error covariance matrix.

It is clear from figure 3 that the parametric uncertainty in the estimated model (11) is relatively large, partly because the model is of quite a high order compared with other, more parametrically efficient models that are discussed in the next section 3.2. In addition to this relatively high order, the main problem with the model (11) is that the interesting sinusoidal behaviour is associated with the initial condition response and it would be preferable is this was integrated with the main TF is some manner.

Given the high order of the above common denominator model, it makes sense to investigate a TF model without this restriction, using the rivcdd routine in CAPTAIN. This yields the following reduced order model characterized by 8 parameters in the continuous time TFs and 2 in the AR(2) noise model. Note that the model is presented here in a decomposed form so that the output of the main TF is denoted by $x_1(t)$ and the output of the initial

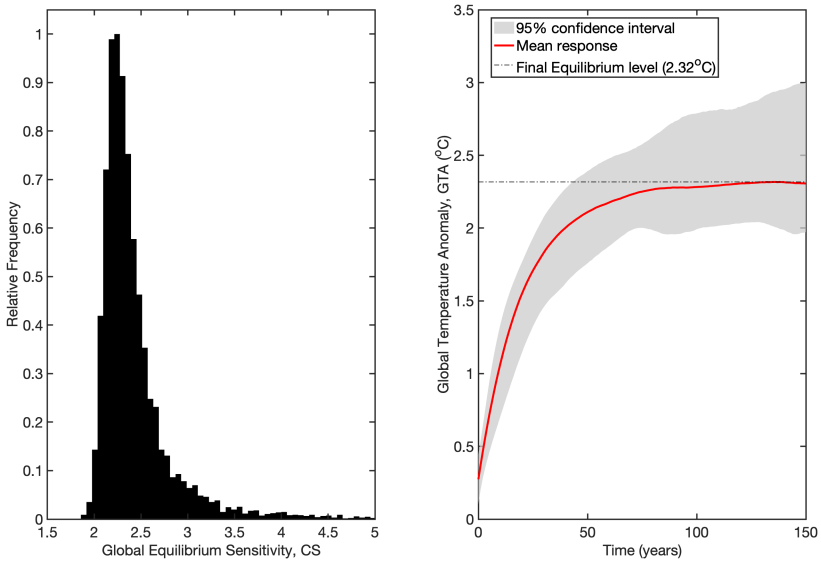

Figure 3: Uncertainty in derived parameter $\hat{\text{ECS}}$ obtained by MCS analysis and the associated response to a 3.7 W/m^2 step change in the total radiative forcing input.

condition TF denoted by $x_2(t)$.

$$\begin{aligned} x_1(t) &= \frac{b_{01}s + b_{11}}{s + a_{11}}u(t) \\ x_2(t) &= \frac{b_{02}s^2 + b_{12}s + b_{22}}{s^2 + a_{12}s + a_{22}}u_{IC} \\ \xi(k) &= \frac{1}{1 + c_1 z^{-1} + c_2 z^{-2}} + e(k) \qquad e(k) = \mathcal{N}(0, \sigma^2) \\ y(k) &= x_1(k) + x_2(k) + xi(k) \end{aligned} \tag{13}$$

where,

$$\begin{aligned} &\hat{a}_{11} = 0.0808(0.012)\ \hat{b}_{01} = 0.0986(0.0094)\ \hat{b}_{11} = 0.0458(0.0013) \\ &\hat{a}_{12} = 0.0319(0.028)\ \hat{a}_{22} = 0.0136(0.0059)\ \hat{b}_{02} = -0.209(0.037) \\ &\hat{b}_{12} = 0.0148(0.0056)\ \hat{b}_{22} = -0.00071(0.00012) \\ &\hat{c}_1 = -0.291(0.079)\hat{c}_2 = 0.167(0.079)\ \hat{\sigma}^2 = 0.0079 \end{aligned} \tag{14}$$

The explanation of the data is marginally less, with $R_T^2 = 0.896$ than in the case of the model (11) ($R_T^2 = 0.900$) but this is obtained with 6 less

parameters. As a result, all of the parameters are estimated with acceptable standard errors. The model response is similar to that shown in figure 2: the main difference is that the sinusoidal initial condition response, with a natural period of 53.7 years is noticeably more damped, as reflected in the larger damping ratio $\zeta = 0.014$. Referring to equation (13), the steady state gain $G = 0.0458/0.0808 = 0.57$, so that the estimated global sensitivity $CS = 3.7 * G = 2.095$, with the time constant $T = 1/0.0808 = 12.4$ years.

3.2 Final Model Identification and Estimation

In the model (11) the oscillatory component in the model is stimulated by the initial condition input u_{IC}. In Young (2018), it is noted that the residual noise in a model that is closely related to that considered in the previous subsection, contains a quasi-cyclic component and it then develops a model for this using a time variable parameter *Dynamic Harmonic Regression* (DHR) model using the dhr routine in CAPTAIN. This model is very effective in forecasting the quasi-cyclic component and predicting the 'levelling' in global warming that occurred after the start of the Millennium and lasted for over 10 years. The equivalent signal in the model (11) is the series $\epsilon(k) = y(k) - x_1(k) = x_i(k) + e(k)$ which is the noisy measure of the initial condition response.

Figure 4 shows that the long term cycle in this $\epsilon(k)$ series, shown in black, can be captured by the following model between the radiative forcing $u(t)$ and $\epsilon(t)$:

$$\epsilon(t) = \frac{b_{01}s + b_{11}}{s^2 + a_{11}s + a_{21}} u(t - \tau) \tag{15}$$

where the associated noise model is an AR(2) process. It will be noted that, in addition to the TF, the relationship requires the introduction of a large pure time delay $\tau = 18$ years between the input and its first effect on the output $\epsilon(t)$. The identification of this model allows for the effect of the τ on the statistical degrees of freedom (because the presence of the time delay reduces the amount of data used in the identification). The estimates of the parameters are as follows, with the standard errors shown in parentheses:

$$\begin{aligned} &\hat{a}_{11} = 0.0158(0.012);\ \hat{a}_{21} = 0.0132(0.0008);\ \hat{\tau} = 18\ years \\ &\hat{b}_{01} = 0.00272(0.0045);\ \hat{b}_{11} = -0.00024(0.00030); \\ &\hat{c}_1 = -0.301(0.083);\ \hat{c}_2 = -0.231(0.083);\ \hat{\sigma}^2 = 0.009 \end{aligned} \tag{16}$$

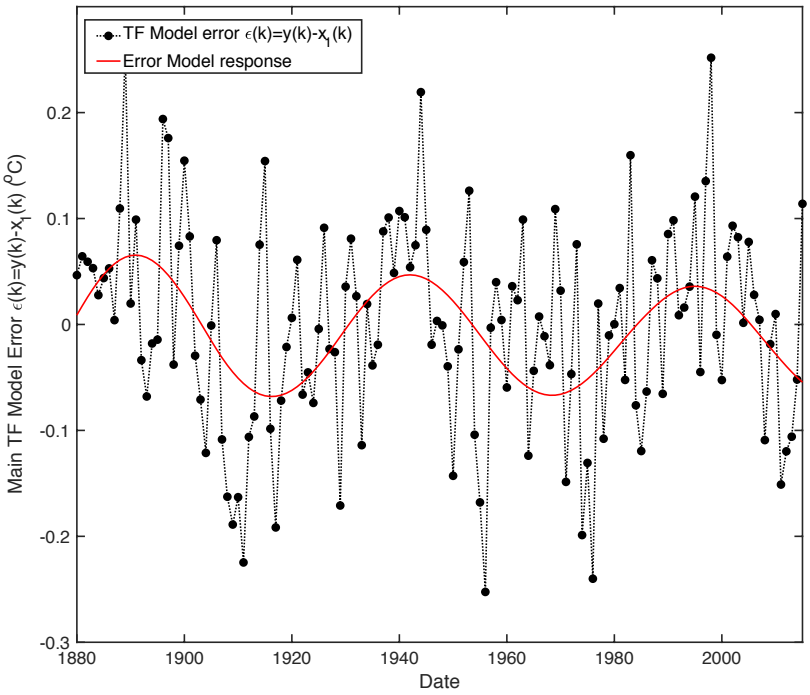

Figure 4: The output of the model (15) compared with the error signal $\epsilon(t)$.

This second order model has a natural frequency $\omega_n = 0.115$ radians/year, with an associated natural period of 54.7 years. The damping ratio is quite small at $\zeta = 0.0158$ so the associated oscillations a quite sustained, taking about 1000 years to die out. Note that the TF numerator parameters are quite poorly defined, with the estimated standard errors both a little larger that the parameter estimates.

The main disadvantage of the model (15) is that, once again, the initial condition equation is still explaining quite a lot of the oscillatory behaviour. These results suggest, therefore, that a modified model is required; one in which the initial condition equation (11)(ii) is replaced by a combination of an internal model based on (15) and, crucially, a different method of estimating the initial conditions. This development is discussed in the next section 3.2.1.

3.2.1 The final DBM model

In order to remove the need for the initial condition equation and the additional input u_{IC} required for this, the final identification and estimation of the model is carried using a simulated model in the Matlab 'Simulink^{TM}' software application. This has the advantage that the initial conditions can be introduced directly as parameters in the three integrators of the simulated differential equations (see the Simulink diagram in Appendix B). The deterministic equations of the Simulink model, presented in TF form, are as follows,

$$\begin{aligned} x_1(t) &= \frac{b_{10}}{s+a_{11}}u(t) && (i) \\ x_2(t) &= \frac{b_{20}s}{s^2+a_{21}s+a_{22}}u(t-\tau) && (ii) \\ x(t) &= x_1(t)+x_2(t) && (iii) \end{aligned} \tag{17}$$

where it will be noted that the numerator of the $x_2(t)$ equation is now identified to have only one term, $b_{20}s$, showing that $x_2(t)$ is the filtered first derivative of $u(t-\tau)$. The differential equation equivalent of (17), as used in the Simulink diagram, takes the form:

$$\begin{aligned} \frac{dx_1(t)}{dt} &= a_{11}x_1(t)+b_{10}u(t) && (i) \\ \frac{d^2x_2(t)}{dt^2} &= a_{21}\frac{dx_2(t)}{dt}s+a_{22}x_2(t)+b_{20}\frac{du(t-\tau)}{dt} && (ii) \\ x(t) &= x_1(t)+x_2(t) && (iii) \end{aligned} \tag{18}$$

The full DBM model is completed by the following discrete-time equation for the measured GTA, $y(k)$, which is not included in the diagram in order to emphasize the simplicity of the model.

$$\begin{aligned} y(k) &= x(k)+\xi(k) \\ \xi(k) &= \frac{1}{1-c_1z^{-1}}e(k) \qquad e(k)=\mathcal{N}(0,\sigma^2) \end{aligned} \tag{19}$$

This is a first order AR(1) model identified by the AIC and, as required, the model residual series $e(k)$ is both serially uncorrelated and uncorrelated with the TRF input series.

The model is now identified with only 6 parameters, including the time delay, plus the 3 initial conditions on the integrators (the $\frac{1}{s}$ blocks in the diagram). These parameters are estimated in a customized optimization

routine, based on the Matlab optimization routine lsqnonlin, that repeatedly calls the Simulink model, adds a discrete-time equation for the noise model, and minimizes the sums of squares of the resulting residual series $e(k)$. This is referred to as 'prediction error minimization' in the systems and control literature (see e.g. Young, 2011). Initially, the starting estimates for the optimization were selected from the estimated parameters of the previously estimated models. On convergence, the model yields a good explanation of the data ($R_T^2 = 0.898$). The resulting parameter estimates are as follows, where the standard errors are shown in parentheses:

$$\begin{aligned}
\hat{a}_{11} &= 0.0518(0.0053);\ \hat{b}_{10} = 0.0320(0.0032);\ \hat{b}_{20} = 0.0067(0.0057) \\
\hat{a}_{21} &= 0.0082(0.0133);\ \hat{a}_{22} = 0.0129(0.0012) \\
\hat{c}_1 &= -0.220(0.078);\ \hat{\sigma}^2 = 0.008 \\
\hat{IC}1 &= -0.317(0.049);\ \hat{IC}2 = 0;\ \hat{IC}3 = -0.0307(0.036);
\end{aligned} \tag{20}$$

with the estimate of the time delay $\hat{\tau} = 17.52(4.4)$ years that suggests the data are explained better if this is 'fractional' (see Chen and Young, 2019). Once again, as required, the model residual series $e(k)$ is both serially uncorrelated and uncorrelated with both the TRF input and the AMO series.

It is important to note that this analysis shows how crucial it is to consider TRF as the forcing input rather than just its carbon emissions component of the TRF. If the latter approach is used, then the explanation of the GTA data is not so good, with $R_T^2 = 0.872$, and the parameter estimates are not so well defined:

$$\begin{aligned}
\hat{a}_{11} &= 0.06836(0.0303);\ \hat{b}_{10} = 0.04801(0.0206) \\
\hat{b}_{20} &= 0.000005(0.0377);\ \hat{a}_{21} = 0.0058(0.0137);\ \hat{a}_{22} = 0.0115(0.0009) \\
\hat{c}_1 &= -0.367(0.074);\ \hat{\sigma}^2 = 0.009 \\
\hat{IC}1 &= --0.2319(0.093);\ \hat{IC}2 = 0;\ \hat{IC}3 = -0.1072(0.051);
\end{aligned} \tag{21}$$

In particular, they have have much larger standard errors (e.g. a 6 times increase for $\hat{a}_{11}$), with a consequent effect on the estimates of the climate-related parameters. And the estimate of the time delay is effectively indeterminate, with $\hat{\tau} = 19.94(3.45 \times 10^5)$.

The model equations (17) can be converted straightforwardly into the

following alternative form (see section 3):

$$\begin{aligned} x_1(t) &= \frac{G}{1+Ts}u(t) && (i) \\ x_2(t) &= \frac{b_{20}s}{s^2+2\zeta\omega_n s+\omega_n^2}u(t-\tau) && (ii) \\ x(t) &= x_1(t)+x_2(t) && (iii) \end{aligned} \tag{22}$$

This reveals the mechanistically meaningful parameters: G, T, ζ and ω_n, which are, respectively, steady state gain and time constant of the 'main model'; and the natural frequency and damping ratio of the 'additive oscillatory model'. A block diagram of the main deterministic parts model, which may be more understandable to readers who have not used Simulink, is shown in figure 5. The GTA response of the model (17) to the TRF is shown by

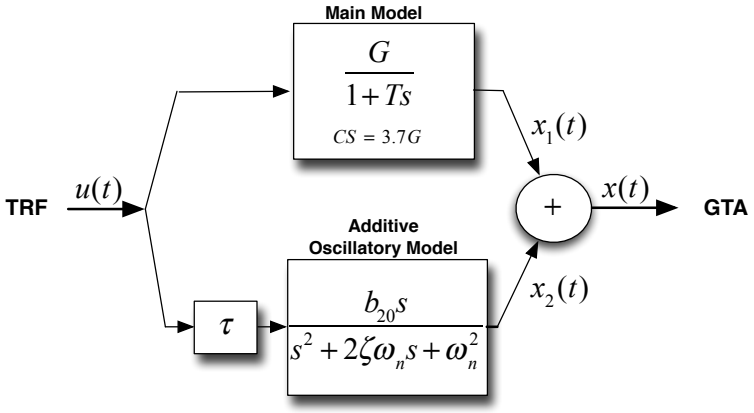

$G = 0.618$; $T = 19.3$ y; $CS = 2.29$; $b_{20} = 0.0067$; $\tau = 17.5$ y

$\omega_n = 0.0181$ c/y; (period 55.3 y); $\zeta = 0.036$

Figure 5: Block diagram of the final DBM model (17).

the full red line in figure 6 Also shown in this figure are the two components $x_1(t)$ (dash-dot red line) and $x_2(t)$ (black line raised by 0.7°C for clarity). Here, the first component $x_1(t)$ is the output of a first order TF. Referring to the previous equations (8) and (9), we see that this TF has a steady-state gain $G = 0.0320/0.0518 = 0.618$ and a time constant $T = 1/0.0518 = 19.3$ years. It is widely accepted that the climate sensitivity is defined as the radiative forcing required for a doubling of CO_2 and this is likely to be about

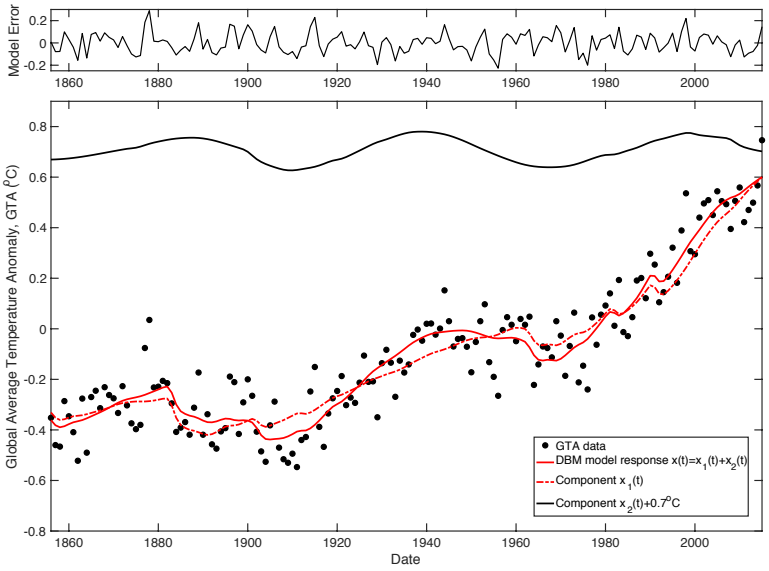

Figure 6: The output of the final DBM model (red full line) compared with the GTA data. Also shown are the component states $x_1(t)$ (red dash-dot line) and $x_2(t)$ (black line), which is raised by 0.7^oC for clarity.

5.35 $log_e(2) = 3.7$ Wm^{-2} (Myhre et al., 1998). Consequently, the climate sensitivity in this case is ECS $= G \times\ 3.7 = 4.15\ ^oC/(W/m^2)$. These parameters define the response of model to a step input of 3.7 $\mathrm{W/m}^2$, as illustrated in figure 7, which can be compared with step response shown in the right hand panel of figure (5) showing the similar step response of the initial model (11), except that the small periodic component is now much larger because the initial condition equation is no longer required (see previous discussion). Note how the oscillations in $x_2(t)$ are: (i) decaying slightly as time progresses because there is no further TRF input to excite them; (ii) have a zero mean value, so that $x_2(t)$ oscillates continually with similar positive and negative excursions about $x_1(t)$; and (iii) that this does not affect the underlying $x_1(t)$ response, nor the final equilibrium level of $x(t)$. Note also the dotted lines in figure,7. These show the response to a 'ramp-step' TRF input, where the initial TRF increases as a slow ramp before levelling at 3.7 $\mathrm{W/m}^2$ after 335 years, revealing how the amplitude of the $x_2(t)$ oscillations are also a function of how the input changes: equation (22) is a stochastic oscillator but the oscillatory output it produces will only be sustained provided there are

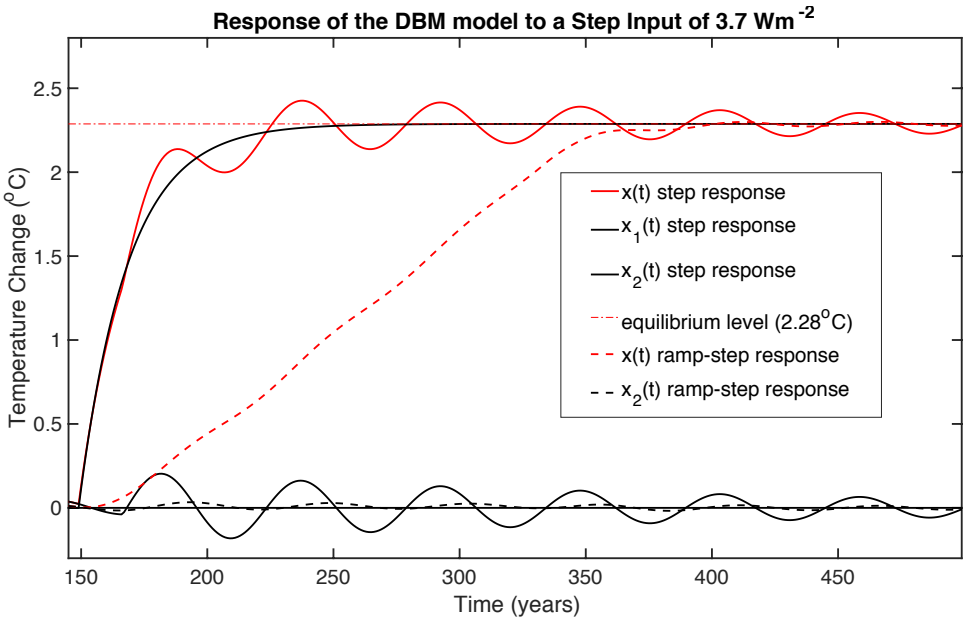

Figure 7: DBM model response to step-like changes in the total radiative forcing input applied after 150 years: (i) a sharp 3.7 W/m^2 step change; and (ii) a much more gentle ramp-step change to the same final level.

sufficient changes in the input to continually stimulate them. This affects the response of the model in hypothetical scenario analysis and forecasting, as discussed later in section 4.

The only parameter in (17) that is not estimated well, with standard error larger than the estimated value, is $\hat{a}_{21}$ (see (31)). Here, the estimated standard error of 0.013 is very much larger than the estimated parameter value of 0.0082, which is extremely close to zero. The implications of this uncertainty on the interpretation of the oscillatory behaviour of $x_2(t)$ in figure 6 are discussed in section 3.7.2. The uncertainty arises mainly because it is the parameter that controls the damping of equation (17)(ii) (see previous equations (8) and (9)), with this very small value making equation (17)(ii) an almost undamped oscillator that explains the sustained sinusoidal response of $x_2(t)$. However, setting it exactly to zero results in a poorer model so, although it is not well defined, this parameter is important to the full model dynamics. In effect, equation (17)(ii) is a stochastic oscillator whose oscillations are maintained by the random perturbations to the system (see also

the first sentence in section 3.5).

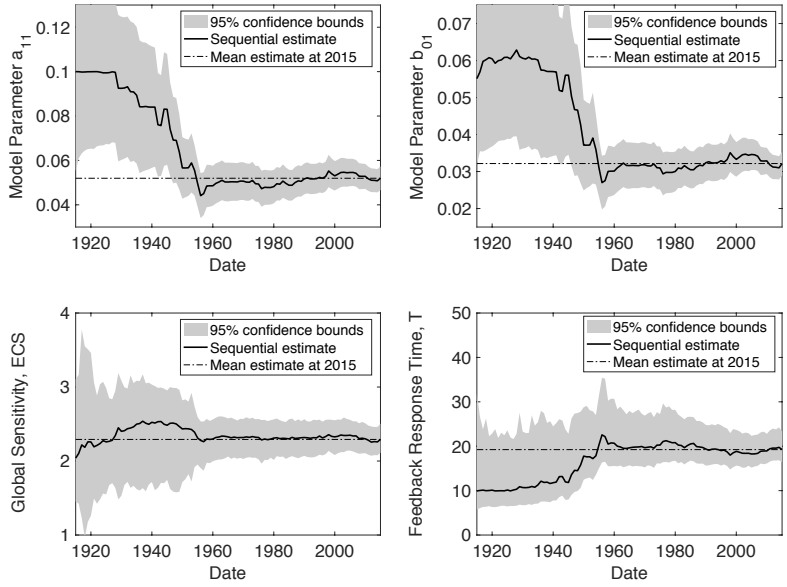

Figure 8: The top two panels show the sequential estimates $\hat{a}_{11}(k)$ and $\hat{b}_{10}(k)$ of the two TF model parameters a_{11} and b_{10} in equation (17)(i). The bottom two panels show the associated sequential estimates of the climate parameter estimates $\hat{\text{ECS}}(k)$ and $\hat{T}(k)$

.

It is often worth considering how well the parameters are converging over time using sequential estimation, where the parameters are re-estimated at every sampling instant based on all of the data up to that sample[7]. The top two panels of figure 8 show the sequentially updated estimates, $\hat{a}_{11}(k)$ and $\hat{b}_{10}(k)$, of the two parameters a_{11} and b_{10} in equation (17)(i) over the period 1915 to 2015, based on data from 1856. These define similar estimates of the two climate parameters $\hat{\text{ECS}}(k)$ and $\hat{T}(k)$ shown in the bottom two panels[8]. Note particularly how the sequential estimates $\hat{\text{ECS}}(k)$ and $\hat{T}(k)$ are

[7]This is an algorithmically inefficient form of recursive estimation (Young, 2011) (which cannot be used with the Simulink model), where the re-estimation involves complete re-optimization at each update.

[8]Note that there are no standard error bounds shown on the bottom two panels in figure 8 because this would have required computationally very expensive MCS analysis at *every* recursive update.

very volatile up to about 1950 but stabilize thereafter for 65 years, showing relatively consistent estimation of these two important climate parameters over this most recent period of time.

It seems likely that this stabilization of the sequential estimates is primarily because the data are more accurate and trustworthy over this period; and also that, after about 100 years, there is then sufficient data to provide a reasonable estimate of the oscillatory component $x_2(t)$. This is confirmed by the similar stabilization of the sequential estimate of the natural period shown in the left lower panel of figure 9. However, bearing upon the discussion

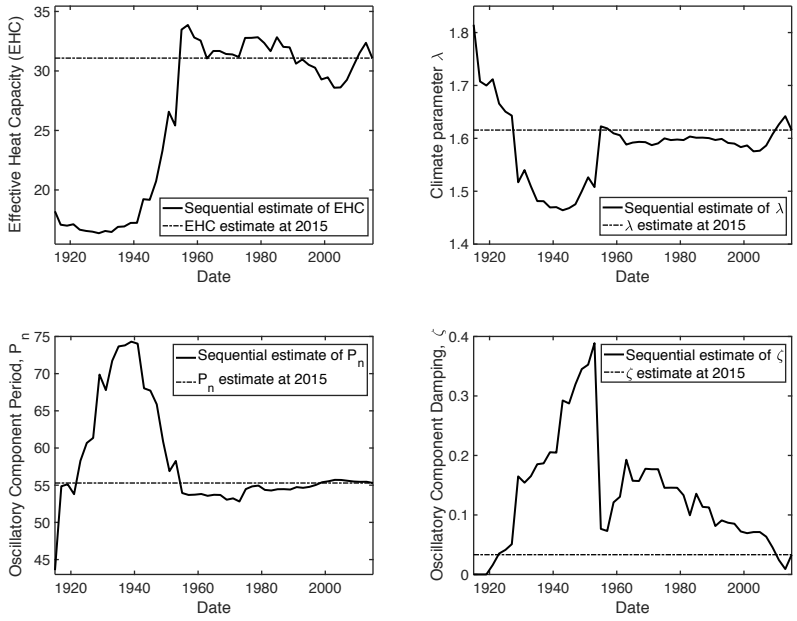

Figure 9: The top two panels show the sequential estimates the climate parameters EHC and λ (see section 3.7.1). The bottom two panels show the sequential estimates of the parameters associated with the oscillatory state $x_2(t)$: the period, P_n, and the damping ratio ζ.

above about the uncertainty in the b_{21} parameter, note how the convergence of the damping parameter ζ, in the lower right hand panel of figure 9, is much more volatile and indeterminate, with no signs of stabilization. The top two panels of figure 9 show that the sequential estimates of the other climate parameters *Effective Heat Capacity* (EHC) and λ, as discussed later in section 3.7.1. Since these parameters are closely related to the estimates

of T and ECS, it is not surprising that they also stabilize well after 1950.

Finally, it is interesting to note the relatively small but noticeable changes in the sequential estimates of these and all of the other parameters that occur after 2000. Presumably, these are associated with the 'levelling' that occurred after the start of the new Millenium (see sections 1, 3.2 and later section 3.7.2).

3.3 Monte Carlo Analysis and Uncertainty

An important aspect of stochastic models is the evaluation of the uncertainty in the parameters and the output response. The optimal estimation procedure yields the error covariance matrix of the directly estimated parameters; and the square root of its diagonal elements provides the estimated standard errors on the parameters shown in equation (31). But the most important parameters in the present climate context are those that have a mechanistic interpretation, most importantly the global equilibrium climate sensitivity ECS and the time constant T, both of which have to be *derived* from the directly estimated parameters.

As in previous sections, the easiest way to estimate the uncertainty in these derived parameters is MCS analysis using the estimated covariance matrix to generate random realizations of the directly estimated parameters that are then entered into the equations for the derived parameters in order to generate realizations for these. As we shall see, such MCS analysis can also involve generating random realizations of the model responses, from which the uncertainty in these responses can be evaluated as 95 percentile bounds.

The main results of the MCS analysis for the DBM model (17)/(18), based on 10000 realisations for the parameters and 5000 for the responses, are presented in figure 10, †figure 11 and Table 2. figure 10 shows the normalized sample distributions of the derived parameters ECS, T and P_n; and the results are summarized in Table 2.

The second panel of figure 11 shows the mean GTA response of the DBM model as a black line, with the 95 percentile bounds shown in grey. For comparison, the simulated response of the estimated model $\hat{x}(t)$ is shown as a red dash-dot line which, as expected, is virtually coincident with the black line. The two lower panels show the mean and 95 percentile bounds for the two components of $\hat{x}(t)$, with $\hat{x}_1(t)$ in the upper panel and $\hat{x}_2(t)$ in the lower panel.

It is clear from these results that the model is statistically well defined

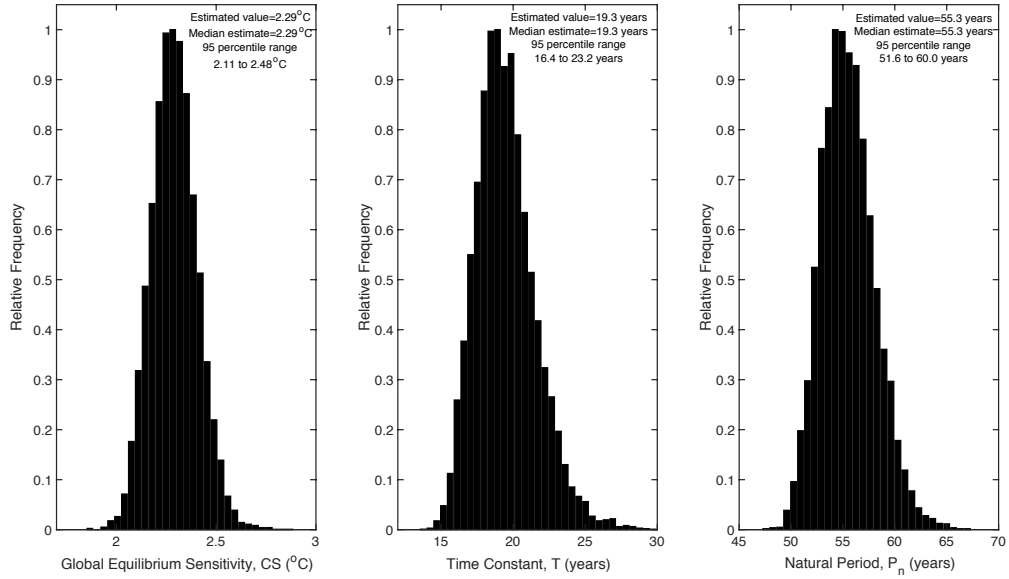

Figure 10: Uncertainty in derived parameters ECS, T and P_n obtained by MCS analysis with 10000 realizations.

Parameter	Estimate	Lower 2.5% Bound	Upper 97.5% Bound
$\hat{\text{ECS}}$ (^{o}C)	2.29	2.07	2.53
$\hat{T}$ (years)	19.3	16.1	24.2
$\hat{P_n}$ (years)	55.3	51.0	61.1
$\hat{\lambda}$ (years)	1.62	1.46	1.79
$\hat{C}$ (years)	31.2	26.1	38.7

Table 2: MCS results for the Final DBM Model based on 10,000 random realizations defined by the estimated error covariance matrix (for definitions of the λ and C parameters, see later section 3.7.1).

and provides a reasonable explanation of the GTA series. The component state $\hat{x}_1(t)$ obviously provides the main and most obvious response to the TRF stimulus. The second component state $\hat{x}_2(t)$ is less obvious but, given the uncertainty in the estimation of long cycle behaviour from short time series, its estimated period of 55.3 years is quite similar to the 62.5 year period associated with the peak in the AR(23) spectrum of AMO series that is considered in the next sub-section.

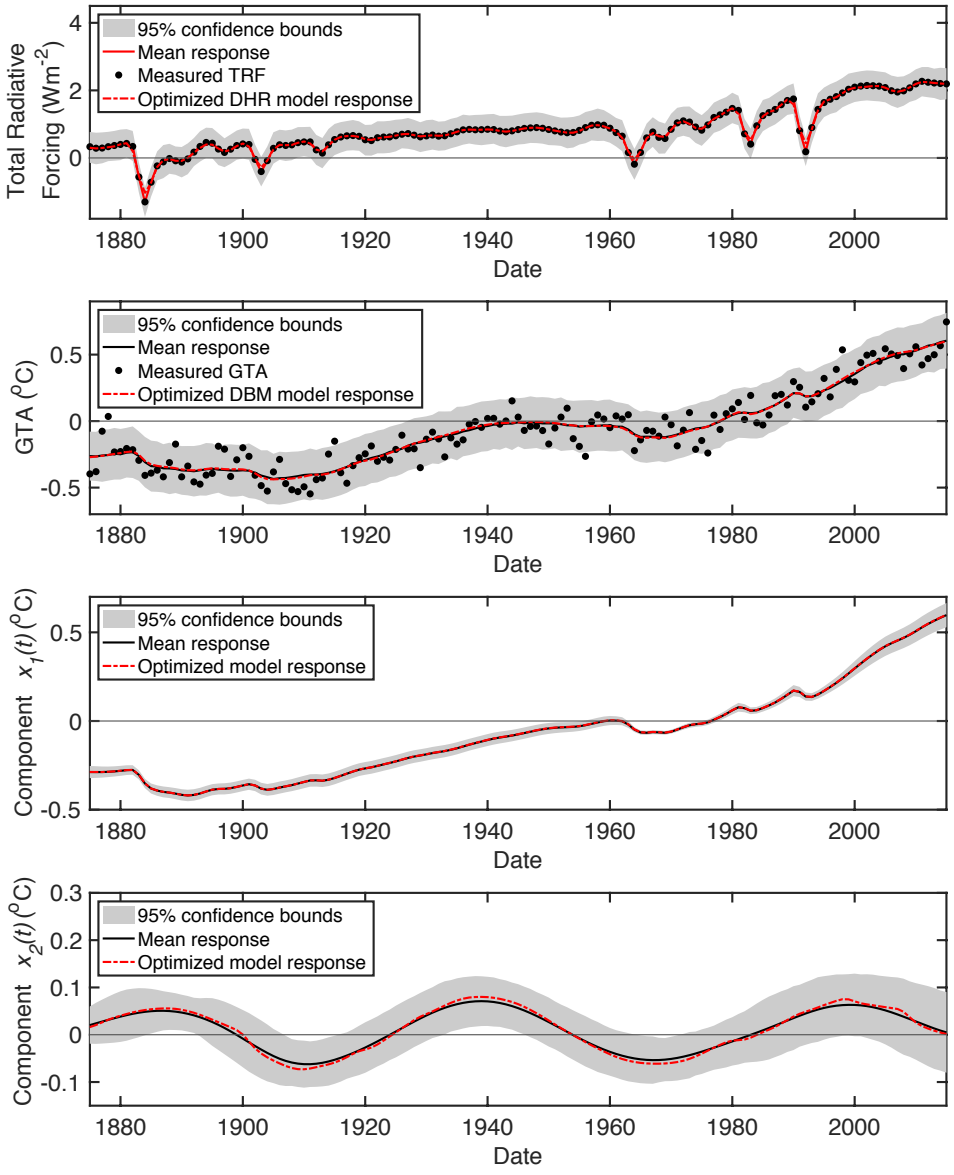

Figure 11: Uncertainty in the responses of $x(t)$, $x_1(t)$ and $x_2(t)$ in the final DBM model, obtained by MCS analysis with 5000 realizations.

3.4 Uncertainty in the TRF

The previous sub-sections have concentrated on the effects of the uncertainty in the DBM model parameters. It is difficult to assess the uncertainty in the

TRF input signal because this is a series constructed by climate scientists based on numerous sources of data. However, in the previous forecasting paper (Young, 2018), a DHR model for TRF was used to forecast its future behavior and its consequent effect on the GTA forecasts. This model includes the estimated uncertainty in the TRF when considered as a univariate time series and this can be utilized to evaluate its effect on the estimation of the DBM model parameters by MCS analysis and compare the estimates of the derived parameters with the those shown previously in Table 2.

DHR modeling of time series (see Young et al., 1999; Young, 2011, for a description of this method) is carried out using CAPTAIN routines and based on the AIC identified autoregressive spectrum of the time series. In this case, the aic routine in CAPTAIN identifies an AR(7) model for the TRF series and the arspec routine is then used to identify the peaks in the AR(7) spectrum that identify the number of terms in the DHR model. The dhropt routine then identifies the optimum hyper-parameters required by the dhr routine (noise variance ratio 'nvr' and 'alpha' parameters that define the *Generalized Random Walk* (GRW) model for the time-variable parameters in the identified DHR model). Finally, the dhr routine uses these optimum hyper-parameters to estimate the components in the DHR model, the sum of which provides the required estimate of the TRF time series.

In the case of the TRF model, there is a long period component, associated with the trend $T(k)$ in the data that represents the main movements of the TRF series; and two main peaks in the AR(7) spectrum that characterize the deviations about $T(k)$. Consequently, the DHR model takes the form:

$$u(k) = T(k) + \sum_{i=1}^{2} \{a(i,k)\cos(\omega_i k) + b(i,k)\sin(\omega_i k)\} + \xi(k) \qquad (23)$$

where the $a(i,k)$ and $b(i,k)$, $I = 1, 2$, are time variable parameters, each modelled as a GRW process; while $\xi(k)$ are the residual errors. The optimized hyper-parameters provided by the dhropt routine are nvr=[0.273 0.763 0.119] and alpha=[0.440 0.857 0.90]. The resulting estimated components from dhr are plotted in the lower panel of figure 12 and, when these are summed together according to equation (23), they produce the model estimate of the TRF series and the associated uncertainty bounds, show in the top panel of figure 12.

Given the DHR model for the TRF, MCS analysis can be carried out where, for each realization, the DBM model is re-optimized using a TRF in-

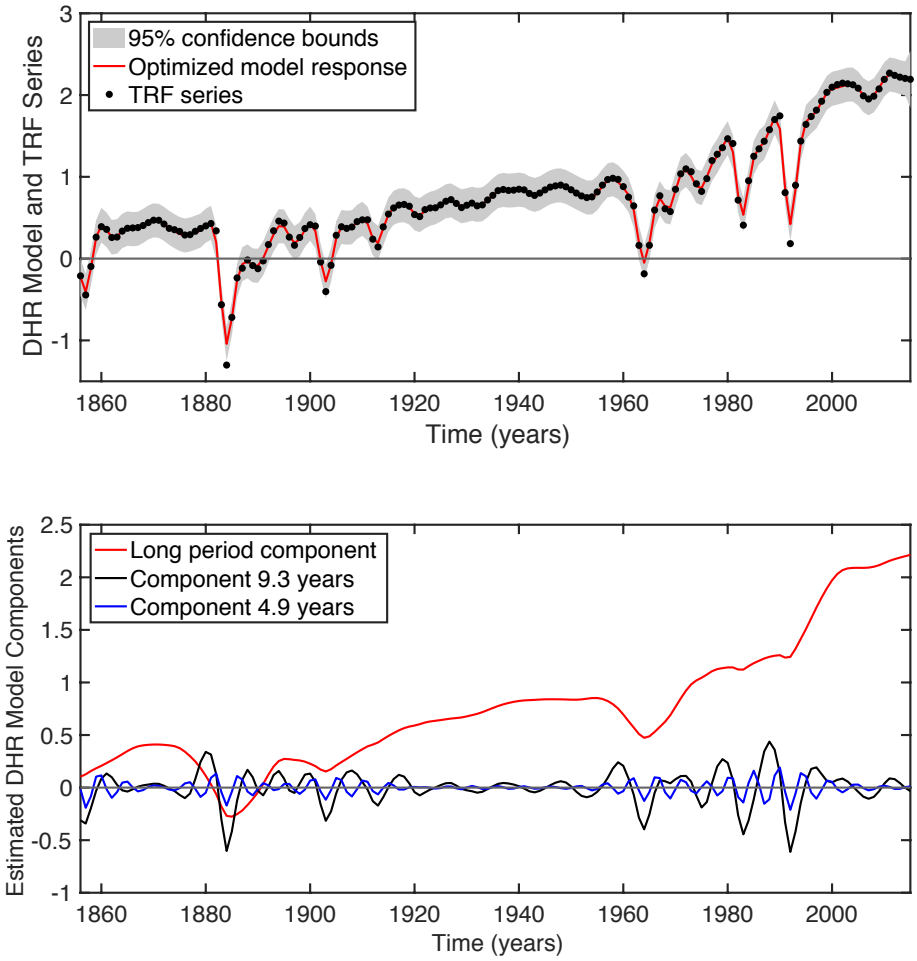

Figure 12: Estimated components of the DHR model for the TRF series.

put based on the DHR model (23), with additive noise based on the estimated uncertainty bounds shown on the top panel of figure 12. This is computationally intensive analysis because of the optimization being required at each realization, so only 1000 realizations are used. The resulting estimates of the derived parameters, shown in Table 3, are very similar to those in Table 2 and justify these previous estimates. The main difference is the confidence interval on the oscillatory state $x_2(t)$, shown in the lower panel of figure 13, which is significantly smaller that in the lower panel of figure 12. This is because the model is optimized for each realization of the MCS analysis, using

Parameter	Estimate	Lower 2.5% Bound	Upper 97.5% Bound
$\hat{\text{ECS}}$ (^{o}C)	2.29	2.07	2.64
$\hat{T}$ (years)	19.9	15.0	26.0
$\hat{P}_n$ (years)	55.5	52.1	58.4
$\hat{\lambda}$ (years)	1.62	1.40	1.82
$\hat{C}$ (years)	32.0	25.6	39.8

Table 3: MCS results for checking the Final DBM Model estimates using additive noise on the TRF. Based on 1000 stochastic realizations

the latest realization of the TRF input; whereas in the earlier analysis, there is only one optimization of the DBM model parameters, using the nominal TRF series as the input, and all the realizations are based on this. This leads to full evaluation of the uncertainty of the parameters of the DBM model and more low-damped realizations of the volatile $x_2(t)$ state that lead to the larger confidence interval. For this reason, it is better to consider the results in figure 12 and table 2 as providing the best estimate of the uncertainty in the DBM model, while the results in figure 13 and table 3 are a check on the reliability of the derived parameter estimates in these earlier results.

3.5 Adding a Model for AMO

Schlesinger and Ramankutty (1994) suggest that there are three possible sources for the AMO signal: (i) random forcing, such as by white noise evoking a coloured signal response; (ii) external oscillatory forcing, such as by a variation in the solar constant; and (iii) an internal oscillation of the atmosphere-ocean system. They reject the first two possibilities and conclude that the most probable cause of this oscillation is an inherent internal oscillation of the atmospheric-ocean system. This seems a reasonable argument and so it makes sense to consider how the AMO oscillations can be modelled in a way that links them with the model (17).

Visually, the quasi-cycle in AMO series has long term oscillatory behaviour that is similar to that of the $x_2(t)$ component of the DBM model (17), with some phase lag. This is confirmed by the cross correlation function between the two series shown in figure 14, where the maximum correlation is a clearly significant 0.61 and there is an obvious lag of several years, Finally, the AIC identified AR(24) spectrum of the AMO, shown in figure 15, is dominated by a peak at a period of 62.5 years. The logarithmic scale is

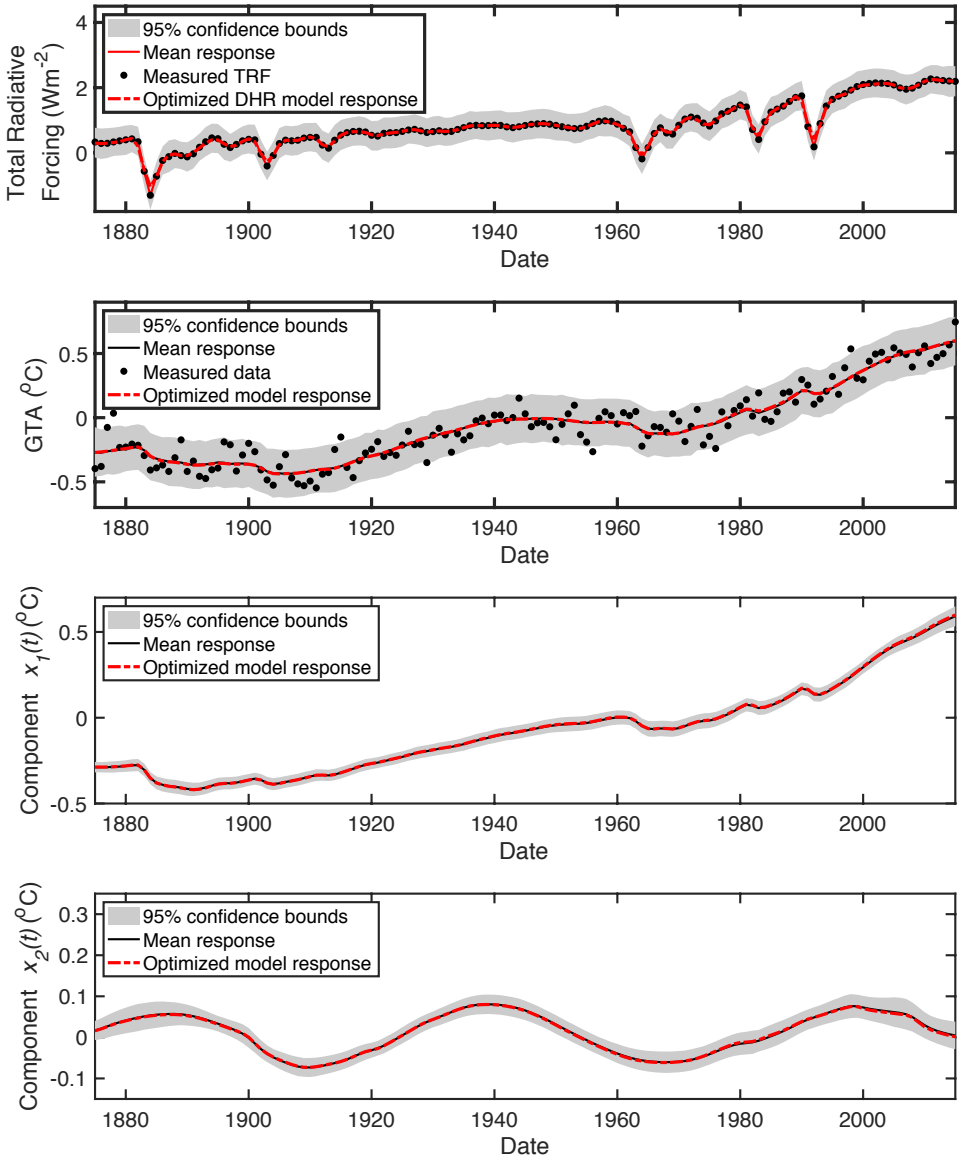

Figure 13: Stochastic simulation results from the final model, including uncertainty on TRF and based on 1000 stochastic realizations

misleading because this is by far the main component. This is revealed most graphically in figure 16, which shows the results of *Dynamic Harmonic Re-*

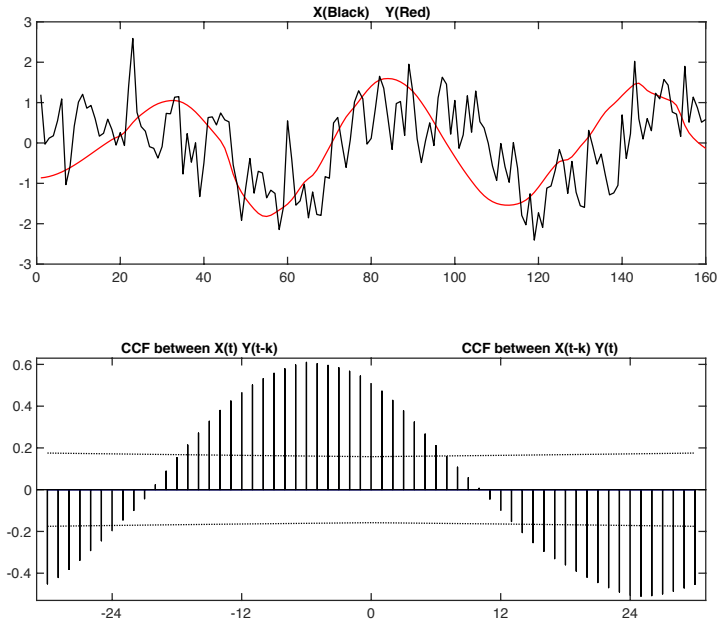

Figure 14: Cross correlation function between the second component state $x_2(t)$ (red line) and the AMO series (blackline).

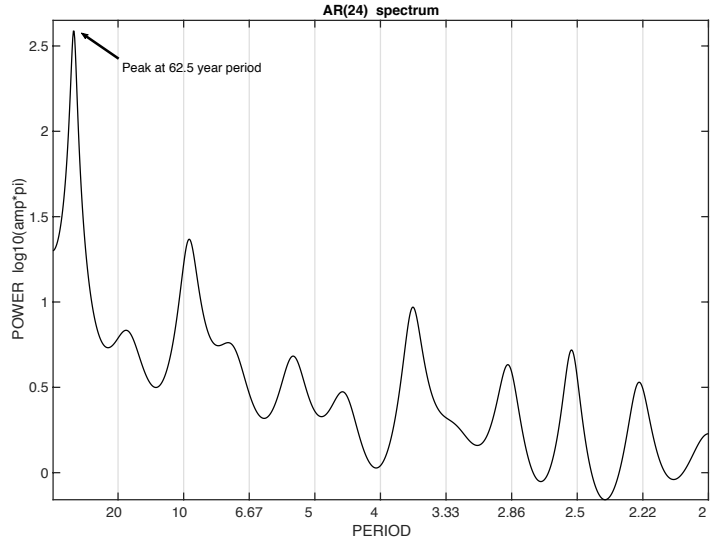

Figure 15: AIC identified AR(24) spectrum of the AMO series.

gression (DHR) analysis based on the AIC identified AR(24) spectrum (see e.g. previous section 3.2). The plot compares the the first component and the sum of the first two components with the AMO series, where the second largest component has a period of 9.6 years. It is clear from this that the first component is predominant, with the second component adding only a small amount to the total. All of the other 9 components are much smaller and can be considered as low level coloured noise. (24).

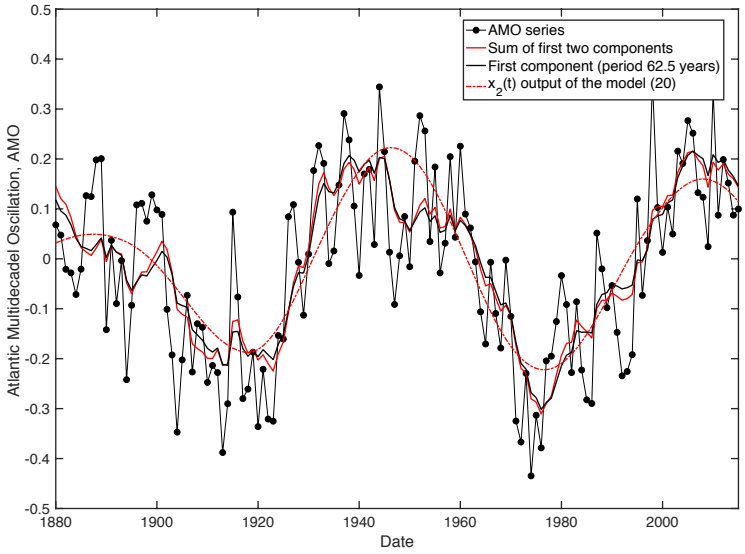

Figure 16: Comparison of the primary component of the AMO signal (black line) with the sum of this and the second largest component (red line) and the AMO series. The red dash dot line is the simulated output of the AMO model (24).

It makes sense, therefore to see if the two series can be related dynamically by a TF model; and the CAPTAIN rivcbjid routine identifies the following [2 2 τ 1 0] model:

$$\begin{aligned} x_3(t) &= \frac{b_{30}s + b_{31}}{s^2 + a_{31}s + a_{32}} x_2(t-\tau) \\ y_3(k) &= x_3(k) + \xi(k) \\ \xi_3(k) &= \frac{1}{1 - c_1 z^{-1}} e(k) \qquad e(k) = \mathcal{N}(0, \sigma_3^2) \end{aligned} \tag{24}$$

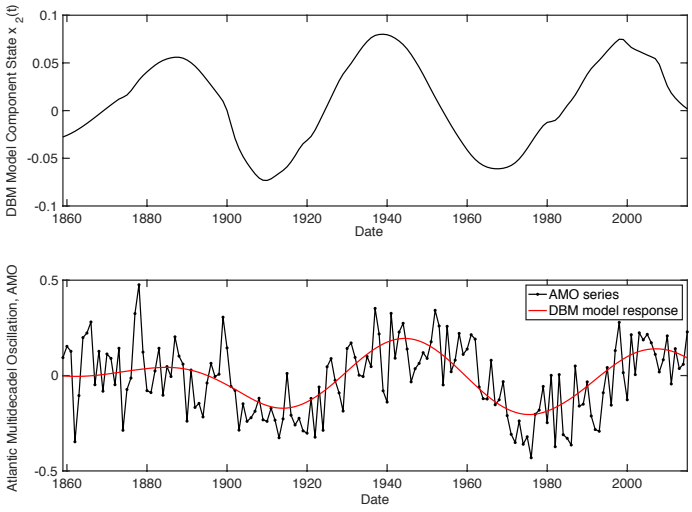

Figure 17: Model between component state $x_2(t)$ (upper panel) and AMO (lower panel) with model response shown as a red line.

where the estimated parameters are as follows, with the standard errors shown in parentheses,

$$\begin{aligned} &\hat{a}_{31} = 0.0031(0.0083);\ \hat{a}_{32} = 0.0047(0.0006);\ \hat{b}_{30} = 0.0806(0.036) \\ &\hat{b}_{31} = -0.0140(0.0032);\ \tau = 2 \text{ yrs};\ \hat{c}_1 = -0.379(0.074); \sigma_3^2 = 0.013 \end{aligned} \tag{25}$$

This model explains the AMO series reasonably well, with $R_T^2 = 0.52$, as shown in figures 16 and 17.

The model (24) has a natural frequency $\omega_n = 0.011$ cycles/year (period 91.5 years) and low damping ratio $\zeta = 0.023$. However, it can decomposed by standard block diagram algebra, using the CAPTAIN routine TFdecomp, into the feedback connection of first order TFs shown at the bottom of the Simulink diagram figure 28, where $a = 0.1772;\ b = -0.0806;\ c = 0.4413;\ d = -0.1741$. This means that the TF in the upper, forward pass TF is a stable first order TF with steady state gain of 0.455 and time constant of 5.64 years; but the lower, positive feedback TF is an unstable first order system with steady state gain of 2.54 and time constant of -5.74 years (where the negative sign indicates the time constant associated with the exponential instability).

It is the feedback mechanism that leads to the low damped oscillatory nature of the model. It seems unlikely, however, that the feedback decomposition has any direct physical interpretation in this case, it is simply showing

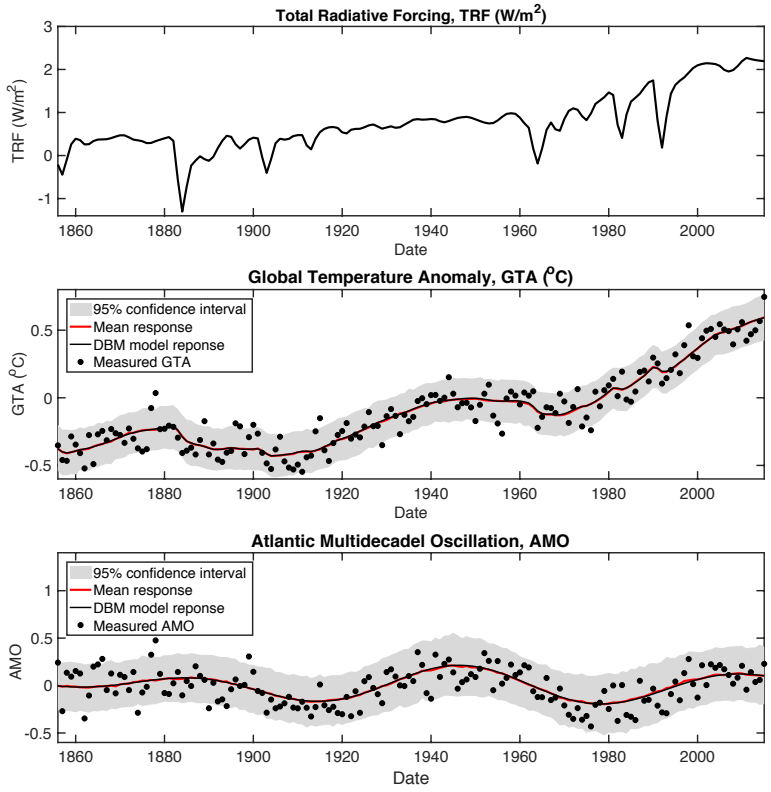

Figure 18: Stochastic simulation results from the final model described by equations (17) and (24), based on 5000 stochastic realizations.

that the two variables can be related dynamically. But this is discussed further in section 3.7.3.

Finally, figure 18 shows the results from the full DBM model, i.e. the combination of the model (17) and the above AMO model TRF, which is the only forcing input to the model, is plotted in the top panel. Below this are plots of the deterministic model outputs and the 95% bounds on these obtained from the results of Monte Carlo analysis, based on the uncertainty in the model parameter estimates and the identified noise on the observations. The model GTA response is compared with the measured GTA in the middle plot; and the model AMO response is compared with the measured AMO in the lower panel. This AMO response is generated from the internally generated cyclic variable through the identified second order system (24), so again this AMO response derives only from the TRF input.

3.6 How accurate are the ECS Estimates?

The previous sections have yielded estimates of the main climate parameters: most importantly in the present context, the global sensitivity and the main time constant, as well as the uncertainty in these estimates. It is important to realize, however, that these estimates are based on only 160 annual measurements of the TRF, GTA and AMO. Given this limited data size, therefore, it is important to consider whether these estimates of the climate parameters can be considered reliable.

In order to get some insight into the nature of parameter estimates for small sample sizes, a Matlab version of the MAGICC emulation model (see Young, 2018, 2019)[9], *which has a known global equilibrium sensitivity* $ECS = 4.17^oC$, has been used to simulate data that is then used to estimate the climate parameters. Figure 19 shows the data generated in this manner.

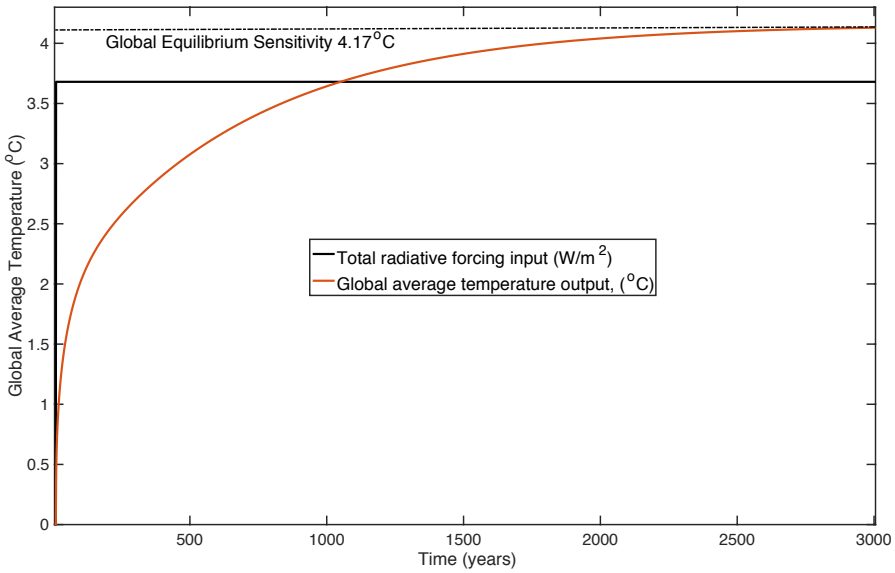

Figure 19: Response of the MAGICC model to a 3.7 W/m^2 step change in total radiative forcing.

The black line is a step input change of 3.7 W/m^2 in the TRF, while the red

[9]This recently updated report cited here can be downloaded from `http://captaintoolbox.co.uk/Captain_Toolbox.html/Publication_Downloads.html` as `HIDBM_Climate2.pdf`.

line shows the response of the MAGICC model to this input stimulus. The step input is used here because it is known to excite dynamic response at all frequencies and so should be 'sufficiently exciting' for the present purposes, although it is not 'persistently exciting' (see the discussion on this in section 8.6.4 of Young, 2011) .

Using the input-output data in figure 19, with a small amount of coloured noise added to the output series to give it some resemblance to reality, 5th order continuous-time TF models were estimated recursively over a progressive range of observation intervals, from a starting point at sample 160 years, then every subsequent year, up to 3000 years, based on all the preceding data. The recursive estimates of ECS and the longest of the five time constants TC, as obtained in this manner, are plotted in the two panels of figure 20. In the left hand panel, we see that that the ECS estimate starts at a

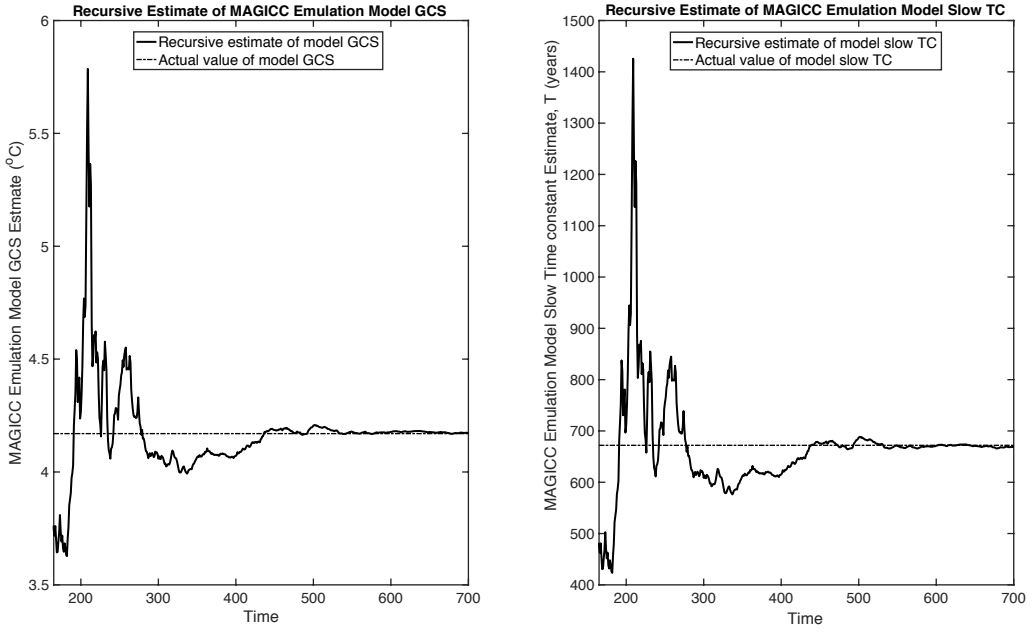

Figure 20: Progressive estimates of the MAGICC model global equilibrium climate sensitivity ECS (left panel) and the slowest time constant, TC (right panel).

value of 3.7^{o}C is then very volatile at first but finally reaches the true value of ECS=4.17^{o}C after about 550 years. Similarly, the estimate of TC starts around 450 years and eventually reaches a relatively stable estimate of 672

years, again after about 550 years. In both cases, reasonably acceptable estimates of the parameters are available after about 440 years but for data size less than this, the estimates are very volatile.

These simulation results show that the information content in the data up to about 440 years of its transient behaviour is not sufficient to reveal with any accuracy the long term characteristics of this simulated system, on which the estimation of the global equilibrium sensitivity depends. In this regard, figure 20 can be compared with figure 8 in section 3.2, which shows that the estimates of the same climate parameters associated with the DBM model (17). These appear to have converged reasonably after 94 years in 1950, or about 59% of the total 160 year sample size, where the estimated time constant is about 19 years, and there is not very much change after this. This convergence is similar to that in the case of the MAGICC emulation model where similar convergence has occurred after 450 years, for a total sample size of 700 years, or 64% of the total, where the estimated time constant about 680 years.

Given the above results, it can be assumed that the estimate of ECS = 2.29^oC, as provided by the DBM model (17), represents a reasonable estimate of the climate sensitivity in 2015, *based on the available globally averaged climate data up to this date*. Although such DBM models are able to forecast very well in the short to medium term (see the forecasting results in Young, 2018), it should not be assumed that they can *reliably* predict the very long term behaviour of the climate system, *as emphasized in this reference*. This is not, however, a real disadvantage of the DBM models because, unlike the more classical climate AOGCM models, they are intended mainly to be used in forecasting, control and climate management applications that relate to the short or medium term (i.e., no more that about 50 years or so into the future).

Of course, it is important to emphasize that, if there is a possibility that the ECS is not reliably estimated on the basis of the available globally averaged data using the parametrically efficient models used in this report, it is almost certainly not identifiable on the basis of any currently available data at the global level. Consequently, any cited estimates of the ECS should be treated with some circumspection. Certainly, it is not wise to make hypotheses about future surface temperatures in the longer term based on such estimates. Moreover, it is unlikely, considering the historical evidence that is available about the past climate, that such equilibrium conditions will ever be achieved: the climate has clearly changed in the past and it is likely that

it will continue changing into the future.

3.7 Mechanistic Interpretation of the DBM Model

An important part of the DBM approach to modelling is the requirement that the identified model can be interpreted in physically meaningful terms and is not just a 'black-box' model that does no more than explain the available data in a statistically satisfactory manner. This section considers, therefore, the two parts of the DBM model (17) in turn: first, the easily interpretable equation (17)(i) relating the total radiative forcing to the changes in global average surface temperature; and second, equation (17)(ii), which is much less easy to interpret. Finally, the additional TF model (24) describing the relationship between the second oscillatory state $x_2(t)$ and the AMO variable is considered in subsection 3.7.3.

3.7.1 The Main model: State $x_1(t)$

The mechanistic interpretation of the main first order TF in equation (17)(i) of the DBM model is straightforward and has been discussed in previous sections. In particular, it is a first order TF with a steady state gain $G = 0.618$ and time constant $T = 19.3$ years. The *Climate Sensitivity*, ECS is defined as the equilibrium temperature achieved by this model when subjected to a doubling of CO_2, which is equivalent to an increase in radiative forcing of $3.7W/m^2$. Consequently, ECS $= 3.7G = 2.29^oC$ and, as we have seen in Table 2 of section 3.3, the 95% uncertainty range on this estimate is 2.11 to 2.48 ^oC. The same uncertainty range for the time constant T is 16.5 to 23.2 years about the mean value of 19.3 years.

But how can the physical nature of the model be interpreted? A simple energy-balance model of the climate system temperature response to changes in radiative forcing that has been suggested a number of times in the climate literature (see e.g. Andrews and Allen, 2007) is the following first order differential equation:

$$C\frac{dT(t)}{dt} = F(t) - \lambda T(t) \tag{26}$$

or in TF terms:

$$T(t) = \frac{\frac{1}{C}}{s + \frac{\lambda}{C}}F(t) \tag{27}$$

where C is a constant *Effective Heat Capacity* (EHC) per unit area; $T(t)$ is the change in the the global-mean surface temperature; $F(t)$ is the TRF; and the constant λ represents 'feedback processes' within the global climate system. This equation can be compared directly with $(17)(i)$ and we see that $C = 1/b_{10} = 31.2$ and $\lambda = Ca_{11} = a_{11}/b_{10} = 1.618$. In the context of the present paper, the steady state gain $G = \frac{1}{\lambda}$ and the time constant $T = \frac{C}{\lambda}$, which Andrews and Allen call the *Feedback Response Time* (FRT).

One advantage of the present analysis, in relation to that of Andrews and Allen, is that we are able to evaluate the uncertainty in the EHC and λ parameters estimates and the MCS generated distributions for these parameters are shown in figure 21, where we see that the 95 percentile range of the EHC per unit area is from 24.8 and 36.7, while that for λ is from 1.38 to 1.92. The figures can be compared with those obtained from Table 1 of Andrews and Allen that presents these measures using data from a set of 18 AOGCMs used in the IPCC Working Group 1 Fourth Assessment Report, Chapter 8 (Randall et al. (2007)). The mean and two standard deviations (95% bounds) for the ECS are 2.95(1.92); and for T are 30.3(17.4), which can be compared with the above DBM model results which, in the same format, are 2.29(0.74) and 18.4(5.8).

Finally, it is worth noting the similarity of the above models and those obtained using the DBM approach for modelling the climate in agricultural buildings (see e.g. Price et al., 1999; Young et al., 2000). In this case, the models are obtained from data collected in *planned experiments* using a large, instrumented chamber that allowed for validation of the model; a procedure that is not, of course, possible in the present context, where we are limited to the analysis of data collected during the normal functioning of the global system.

This study of mass and energy transfer in the chamber showed that a simple first order equation of this same kind (see equation (9) in Price et al., 1999) was able to accurately model the changes in temperature and absolute humidity at any location in the chamber, a well as demonstrating the imperfect nature of the mixing. In particular, it was found that the concept of an *Active Mixing Volume* (AMV), developed by Young and Lees (1993) was applicable to the chamber, with the AMV and the associated *Dispersive Fraction* (DF: the ratio of the AMV to the total volume of the chamber) quantifying the level of the *imperfect mixing*, with DF values considerably less than 0.5, so that the volume of air actively involved in mixing was less than half of the chamber volume, with the rest composed of 'dead-zones'

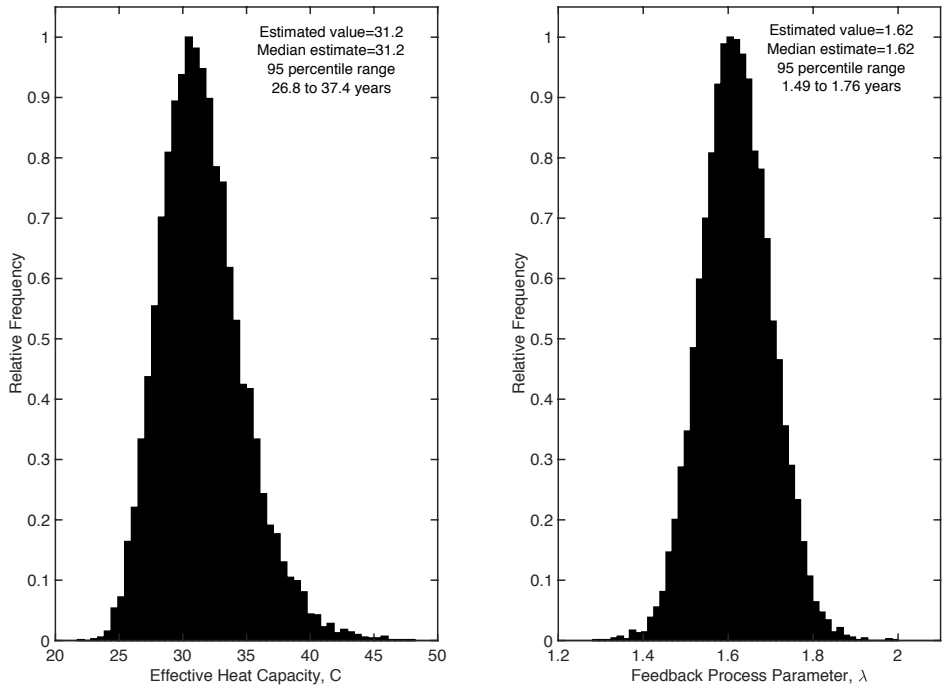

Figure 21: Uncertainty in derived parameters C and λ obtained by the MCS analysis.

(Beer and Young, 1983).

This same type of AMV model has also been used successfully to characterize imperfect mixing process that dominate solute transport in rivers and soils (Beer and Young, 1983; Wallis et al., 1989; Beven and Young, 1988; Young and Wallis, 1993), as well as the micro-climate of horticultural glasshouses Young et al. (1994). It seems reasonable, therefore, that a similar AMV interpretation can be applied to simple climate models, such as those above.

More nteresting from the current climatic perspective, however, the DBM model of the chamber was identified from the experimental data as a second order system; one that could be decomposed into a feedback connection of two first order systems with quite different time constants (where the time constant is defined in this context as the ratio of the AMV to the air flow rate). In particular, the system in the feedback path had a much longer time constant that had not been identified at all during the previous model for-

mulation. This previous analysis had employed a conventional hypothetico-deductive approach, based on standard heat transfer theory, in which the chamber was considered as a single 'mixing box', with a volume equal to that of the whole chamber (i.e complete mixing).

It was established that the additional feedback mode of heat transfer in the chamber related physically to a 'double-glazing' buffer zone constructed around the chamber in order to minimize the disturbance of airflow within the chamber by heat conduction *from the laboratory*. This was incorporated during the construction of the chamber but not thought to affect the heat transfer from this buffer zone *into* the chamber very much and so it was not considered in the model.

As we shall see in the next sub-section 3.7.2, there is a clear analogy here with a feedback decomposition of the oscillatory mode TF in (3.2.1)(*ii*), a mode of behaviour that has not, apparently, been included in climate models heretofore and can be interpreted, hypothetically, in terms of heat energy transfer between the atmosphere and the ocean.

3.7.2 The Main Model: Oscillatory State $x_2(t)$

As pointed out in section 3.2, the oscillatory state $x_2(t)$ has an estimated period of 55.3 years, with a 95 percentile range between 51.6 and 60 years. Most significantly in climatic terms, the recession periods of this oscillation coincide and, therefore, are used in the model, to explain the climate shifts ('pauses' or 'levelling') in the generally upward trend of the GTA.

The potential importance of quasi-cyclic behaviour with a period of around 50-70 years has been known for some time. For example, **?** applied singular spectrum analysis to four global-mean temperature records and identified a temperature oscillation with a period of 65-70 years. They concluded that

> "the 65-70-year oscillation is the statistical result of 50-88-year oscillations for the North Atlantic Ocean and its bounding Northern Hemisphere continents. These oscillations have obscured the greenhouse warming signal in the North Atlantic and North America. Comparison with previous observations and model simulations suggests that the oscillation arises from predictable internal variability of the ocean-atmosphere system".

Moreover, as discussed in the next section 3.7.3, the AMO variable and other multidecadel oscillatory phenomena that have been measured by cli-

mate scientists, could be redolent of a complex internal energy exchange mechanisms that are giving rise to significant quasi-cyclic behaviour in the ocean-atmosphere system that may be related to the oscillatory $x_2(t)$ state variable.

Some insight into the nature of the $x_2(t)$ model can be obtained by looking once more at the second order TF model (18)(ii). As in the case of the experimental chamber discussed in the previous sub-section and the AMO model in section 3.5, this model can be decomposed into the feedback connection of two first order TF components, as shown in figure 22. This can

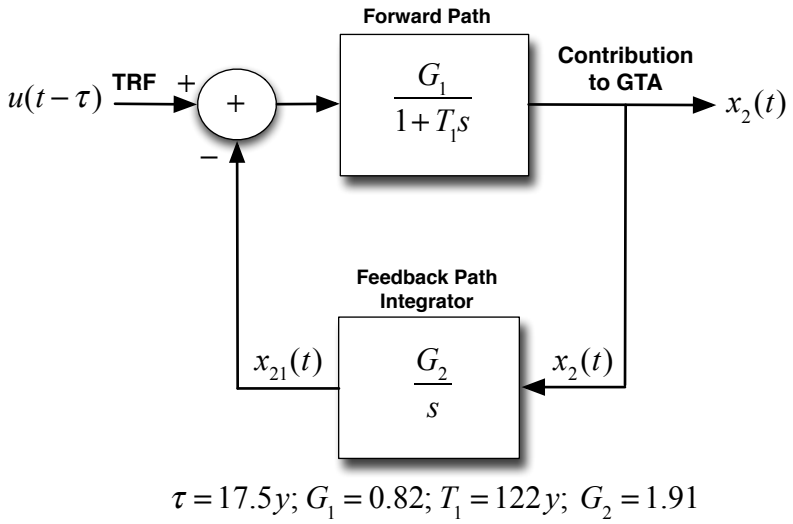

Figure 22: Decomposed block diagram of the model for $x_2(t)$.

be represented alternatively in the following state space form:

$$\begin{aligned} T_1 \frac{dx_2}{dt} &= -x_2(t) + G_1\{u(t-\tau) - x_{21}(t)\} \\ T_2 \frac{dx_{21}}{dt} &= -x_{21}(t) + G_2 x_2(t) \end{aligned} \tag{28}$$

where $x_{21}(t)$ is the 'feedback path' variable. The estimates of the parameters are:

$$G_1 = 0.8214;\ T_1 = 121.9 \text{ yrs};\ G_2 = 1.913 \tag{29}$$

This is a negative feedback system where the feedback path consists of a simple integrator with gain $G_2 = 0.1.913$, so that the global average temperature

change is having a cumulative effect within this feedback system. The overall effect of this negative feedback mechanism, with the long time constant of 121.9 years in the forward path and the integrator in the feedback path, is to create the oscillatory mode of behaviour that is so important in explaining the subtle oscillatory temperature changes observed in the GTA. In other words, the combination of the gains and time constants in the two boxes is creating some form of heat energy exchanges that promotes the oscillatory nature of the response.

Given no further information, one can only speculate on the physical nature of this oscillatory heat exchange mechanism. The presence of the integrator in the feedback path suggests that this feedback part of the system relates to mixing processes that are very long term, suggesting that these are probably occurring slowly in the global oceanic system, which is accumulating the effects of the changes on the globally averaged temperature. Thus we could consider this interchange of energy between the atmosphere and the ocean, and vice-versa, as a physical process that, over the past 160 years, has sustained the oscillatory movements in $x_2(t)$ and so caused fairly regular, periodic changes in the GTA, one of which caused the levelling in the GTA after the start of the new Millenium.

It is important to stress, however, that the estimates in (29) are not well defined statistically: they are derived from the following estimated parameters in (31),

$$\begin{aligned} &\hat{b}_{20} = -0.000045(0.0006);\ \hat{b}_{21} = 0.00684(0.0058) \\ &\hat{a}_{21} = 0.00885(0.0143);\ \hat{a}_{22} = 0.0128(0.0016) \end{aligned} \tag{30}$$

one of which, $\hat{a}_{21}$, as pointed out previously in section 3.2.1, has a large standard error relative to its estimated value. Indeed, only $\hat{a}_{22}$, which defines the natural frequency and period of the oscillation, is estimated well (t-statistic=8), as shown by the histogram of the period in figure 10. It is not surprising, therefore, that MCS analysis yields unsatisfactory results, with all the parameters in the decomposed model having very large percentile bounds, even when any obvious outliers caused by instability are removed, as shown in Table 4:

Of course, an alternative approach to modelling the system in this decomposed form is to estimate the parameters directly in this form using a similar optimization methodology to that employed in section 3.2.1, with a modified Simulink model including the decomposed TF to generate $x_2(t)$. However,

Parameter	Estimate	Lower 5% Bound	Upper 95% Bound
$\hat{T}_1$ $(years)$	122	30	425
$\hat{G}_1$	0.82	0.04	2.6
$\hat{G}_2$	-1.91	-6.88	-0.81

Table 4: MCS results for the Initial DBM Model based on $10,000$ random realizations defined by the estimated error covariance matrix.

this is not so straightforward because it is found necessary to constrain one parameter and one initial condition (which is poorly estimated and close to zero) in the decomposed TF in order to avoid ambiguity in the estimation (i.e. infinite confidence intervals) and obtain reasonable standard errors on the remaining parameters. For instance, taking the reasonable step of constraining the gain G_1 to be equal to the gain in the main TF (i.e. b_{10}/a_{11}), so that ECS for the oscillatory TF is also the same) yields the following parameter estimates:

$$\begin{aligned} \hat{a}_{11} = 0.0491(0.0049);\ \hat{b}_{10} = 0.0303(0.0029);\ \hat{T}_1 = 150(158) \\ \hat{G}_2 = 2.495(2.083);\ \hat{c}_1 = -0.211(0.078);\ \hat{\sigma}^2 = 0.008 \\ \hat{IC}1 = -0.335(0.0.072);\ \hat{IC}2 = 0;\ \hat{IC}3 = -0.479(1.237); \end{aligned} \tag{31}$$

Even with these constraints, however, we see that the parameters of the decomposed TF (T_1 and G_2) have large standard errors so, although the model explains the data well with $R_T^2 = 0.898$ and obtains an estimate of $\hat{\text{ECS}} = 2.285$ close to the 2.288 of the model (18), it cannot be considered fully satisfactory from an estimation standpoint.

Considering the above results, we can be confident that the oscillatory state is present and playing an important part in explaining the changes in the GTA. Moreover, the decomposition into to the feedback system is unique and the interpretation in this decomposed form, with an integrator in the feedback path, makes good physical sense. However, while the parameters in the oscillatory state equation, except b_{21}, are estimated well in the originally identified model form (18), we see above that this is not the case with the decomposed version of this model and the values of the decomposed system have to be considered with more circumspection. It is clear, therefore, that more research is required to interpret the nature of the heat energy exchanges that are suggested by this decomposed model.

Finally, as regards the estimation of the climate parameters, it should be noted that, while the oscillatory state $x_2(t)$ is important in explaining the

GTA data, its does not affect the estimation of the climate sensitivity ECS because the oscillatory behaviour it introduces has a mean value that is very close to zero, with the positive and negative movements of the oscillations cancelling out in the long term (see also the comments in this regard later, in section 4). Of course, although its variations do nota affect the estimation of the ECS, its presence does lead to differences in the *estimated value* of ECS. For example, if the model is estimated by rivcbj without this oscillatory component, the estimates of the parameters a_{11} and b_{10} (with the standard errors in parentheses) and the associated estimate of the ECS are:

$$a_{11} = 0.0713(0.0144);\ b10 = 0.0421(0.0064); ECS = 2.18 \tag{32}$$

which can be compared with the final model estimates:

$$a_{11} = 0.0518(0.0053);\ b10 = 0.0320(0.0032);\ ECS = 2.29 \tag{33}$$

where it will be noted that the standard errors on the final model are considerably smaller than in the simpler model without the stochastic oscillator equation.

3.7.3 The AMO State $x_3(t)$

The AMO model and its connection with the other components is not easy to interpret in mechanistic terms. The Bode diagram (gain and phase plots vs frequency) suggest that it is most likely that the model could be just adjusting the gain and phase of the $x_2(t)$ signal so that it matches the AMO signal. It is less likely that the feedback decomposition shown in the Simulink digram (see figure 28 in Appendix B) has any physical interpretation. However, the AMO is one of various major climate modes (e.g. others are the *Pacific Decadal Oscillation* (PDO), the *North Pacific Index* (NPI), and the *El Nino/Southern Oscillation* (ENSO)) and these may all be connected in some way. For instance these modes may interact and resonate with each other in a variable manner, so that the oscillatory state $x_2(t)$ in the main DBM model (17) is the product of such interaction, as seen in the global surface temperature changes.

The possibility of interaction and resonance is discussed in Swanson and Tsonis (2009) who conclude that, if the coupling between the modes increases, the existing synchronization could collapse and the climate might emerge in a new regime represented by a shift in the temperature trend. This seems

a reasonable hypothesis if it is assumed that the global system is nonlinear with feedback processes and 'teleconnections'. In which case, we should view the AMO model in equation (24) as simply an explanation of the data over the 1856-2015 period and should not consider this necessarily as behaviour that will continue into in the future.

Nevertheless, the unprejudiced identification of such sustained oscillatory mode, with a period in the 95 percentile range of 51.6 and 60 years, suggests that there is, within the global climate system, a mechanism that is sustaining such cyclic or quasi-cyclic behaviour; behaviour that, if our hypothesis of the a relationship between the oscillatory state $x_2(t)$ and the AMO is correct, is related to the observable changes in the upward trend of global warming. It also suggests that there is a clear and urgent need for more research on this topic that might be able to find a physical explanation for this observed behaviour.

3.8 Other Models

Other linear differential equation models are possible, in the sense that they explain the data well. For instance, given that the models discussed in previous section relate the TRF input to the GTA and the quasi-cyclic changes in the AMO, it is possible to consider the direct modelling of the GTA with three inputs: $u_1(t)$=TRF, $u_2(t)$ =AMO and an input u_{IC} to handle the initial conditions, as in all previous models. Or we could add other inputs, to see if they could help to explain the data better, such as the *Southern Oscillation Index* (SOI), a plot of which is shown in figure 23. The SOI index defines the changes in the *El-Nino-Southern Oscillation* (ENSO), an irregularly periodic variation in winds and sea surface temperatures over the tropical eastern Pacific Ocean, affecting the climate of much of the tropics and subtropics. Taking the SOI into consideration as an additional input $u_3(t)$, the following common denominator model is identified and estimated

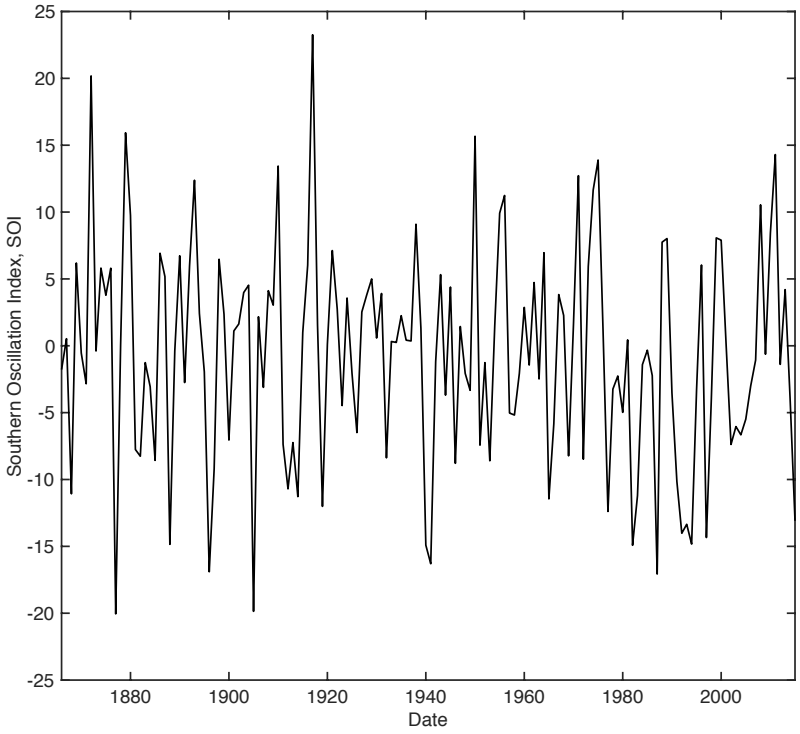

Figure 23: The Southern Oscillation Index, 1866-2015.

using the rivcbjid routine:

$$
\begin{aligned}
x_1(t) &= \frac{b_{01}s + b_{11}}{s + a_{11}} u_1(t-\tau); \\
x_2(t) &= \frac{b_{02}s + b_{12}}{s + a_{11}} u_2(t-\tau) \\
x_3(t) &= \frac{b_{03}s + b_{13}}{s + a_{11}} u_3(t-\tau) \\
y_3(k) &= x_1(k) + x_2(k) + x_3(k) + \xi(k) \\
\xi(k) &= \frac{1}{1 - c_1 z^{-1}} e(k) \qquad e(k) = \mathcal{N}(0, \sigma^2)
\end{aligned}
\tag{34}
$$

where the initial condition equation has been omitted, for simplicity, and the estimated parameters are as follows, with the standard errors shown in

parentheses,

$$\begin{aligned}
&\hat{a} = 0.0254(0.0144);\ \hat{b}_{01} = 0.0535(0.0240);\ \hat{b}_{11} = 0.0201(0.0062) \\
&\hat{b}_{02} = 0.3177(0.0414); \hat{b}_{12} = -0.0022(0.0085); \hat{b}_{03} = -0.0036(0.0007); \\
&\hat{b}_{13} = -0.00086(0.0005); \hat{c}_1 = -0.2526(0.0794); \sigma^2 = 0.0047
\end{aligned} \tag{35}$$

This model explains the data very well with an $R_T^2 = 0.94$ that is somewhat larger than the models estimated in previous sections. However, this is deceptive because the standard errors on some of the parameters are quite large, particularly $\hat{a}_{11}$ which is critical in estimating both the ECS and T estimates using MCS. In fact, the resulting percentile bounds have little meaning unless obvious 'outlier' estimates are removed. Table 5 below was compiled by eliminating all ECS estimates outside the range $0 \rightarrow 15$ and T outside the range $0 \rightarrow 500$. MCS generated estimates of ECS and T together with their 95% bounds are shown in the upper two lines of Table 5; while the results obtained without any outlier removal shown in the bottom two lines.

Treatment	Parameter	Estimate	Lower 5% Bound	Upper 95% Bound
Outliers	$\hat{\text{ECS}}$ (^{o}C)	3.44	2.38	10.50
removed	$\hat{T}$ (years)	64.0	26.1	237.4
Outliers	$\hat{\text{ECS}}$ (^{o}C)	3.44	-4.78	10.78
retained	$\hat{T}$ (years)	64.0	-246.1	340.3

Table 5: MCS results for the model (34) based on $10,000$ random realizations defined by the estimated error covariance matrix.

While the linear models considered in the previous sections, unlike the model (34), are able to explain the data adequately, with statistically well defined climate parameters and reasonable mechanistic interpretations, it is also tempting to consider nonlinear models. However, there are no clear signs of nonlinearity in the data: e.g. the preliminary analysis of the data using *State-Dependent Parameter* nonlinear modelling methods (see chapter 11 in Young, 2011) produced little evidence of state-dependency in the parameters and the explanation of the data was similar to that obtained with the purely linear models. But this does not mean that nonlinear models are not feasible and they provide a possible area of future research (see comments in the next section).

4 Hypothetical Scenario/Forecasting Analysis

Combining the models (17) and (24), the full DBM model can be written as:

$$
\begin{aligned}
x_1(t) &= \frac{b_{10}}{s + a_{11}} u(t) && (i) \\
x_2(t) &= \frac{b_{20}}{s^2 + a_{21}s + a_{22}} u(t - \tau) && (ii) \\
x(t) &= x_1(t) + x_2(t) && (iii) \\
y(k) &= x(k) + \xi(k) && (iv) \\
\xi(k) &= \frac{1}{1 + c_1 z^{-1}} e(k) \qquad e(k) = \mathcal{N}(0, \sigma^2) && (v) \\
x_3(t) &= \frac{b_{30}s + b_{31}}{s^2 + a_{31}s + a_{32}} x_2(t - \tau) && (vi) \\
y_3(k) &= x_3(k) + \xi(k) && (vii) \\
\xi_3(k) &= \frac{1}{1 + c_{1_a} z^{-1}} e(k) \qquad e(k) = \mathcal{N}(0, \sigma_3^2) && (viii)
\end{aligned}
\tag{36}
$$

Although this model has been identified primarily as a model that can be used to obtain estimates for climatically meaningful parameters and their implications on the climate dynamics, it can be used for other purposes. It could be used for short to medium-term forecasting but the adaptive capability of the alternative forecasting model in Young (2014, 2018), probably make it a superior tool in this regard.

One obvious application for the above model (36) is a tool for evaluating possible future globally averaged surface temperature behaviour, based on specified hypothetical emissions scenarios that affect the future behaviour of the TRF input. Figure 25 shows the outcome of a typical exercise of this kind based on the *Representative Carbon Pathway* (RCP) scenarios prepared by the task group 'RCP Concentrations Calculation and Data' in the preparation of the IPCC Fifth Assessment Report (Meinshausen et al., 2011). The four scenarios are defined by four different hypotheses about the future behaviour of the TRF from 2015 to 2500[10]. Figure 24 is a plot of these scenarios, each of which is used as totally deterministic, without any assumptions about its uncertainty into the future. Without such uncertainty, the 95 percentile bounds *are based entirely on the estimated uncertainty in model parameters and measurement noises* $\xi(k)$; and a single realizations of this noise variable

[10]source: `http://www.pik-potsdam.de/~mmalte/rcps/`

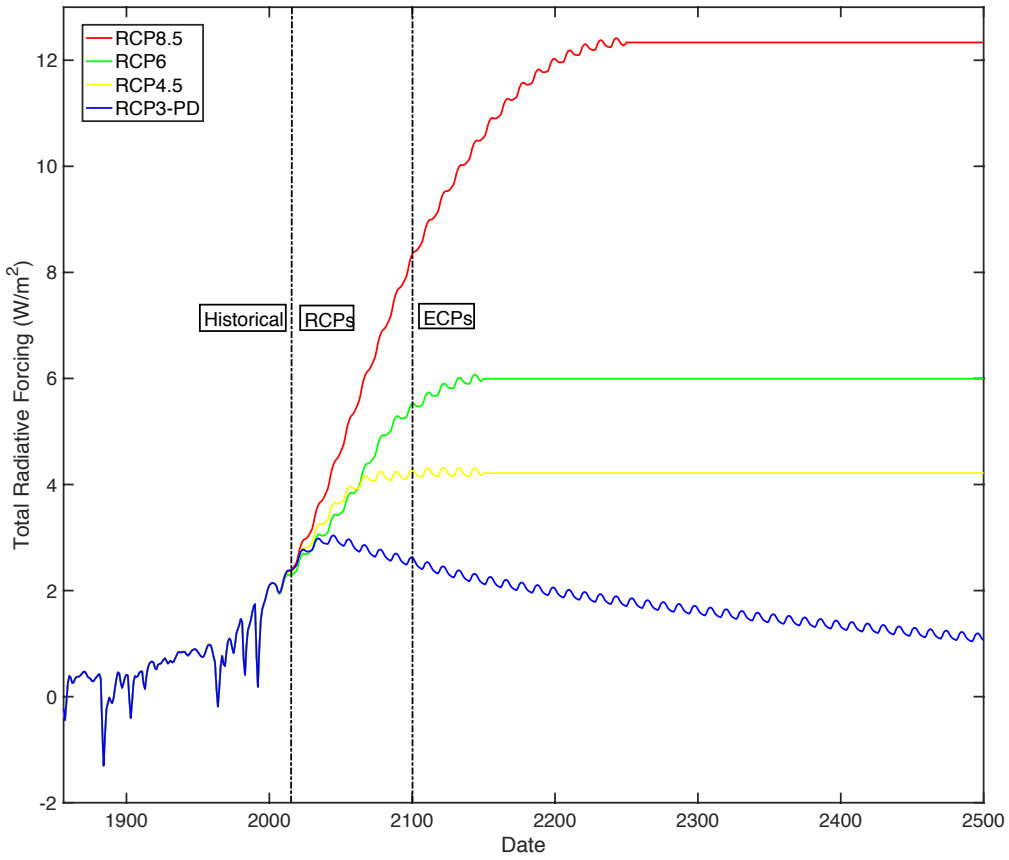

Figure 24: The four *Representative Carbon Pathway* (RCP) scenarios used for the analysis shown in figure 25.

is added to the simulated model output for scenario RCP3-PD after 2015, in order to illustrate its effect. The 95% bounds are useful for illustrating the uncertainty arising from the model alone and are presented here for this purpose.

Of course, the confidence bounds would be much larger if the considerable uncertainty associated with the future TRF was also taken into account, as in short to medium term forecasting and control (emissions management) applications, such as those discussed in (Young, 2006; Jarvis et al., 2008). An application of this type that is similar to scenario analysis is 'hypothetical' forecasting, which investigates the possible future behaviour of the GTA that might result from forecast changes in the TRF and its associated uncertainty

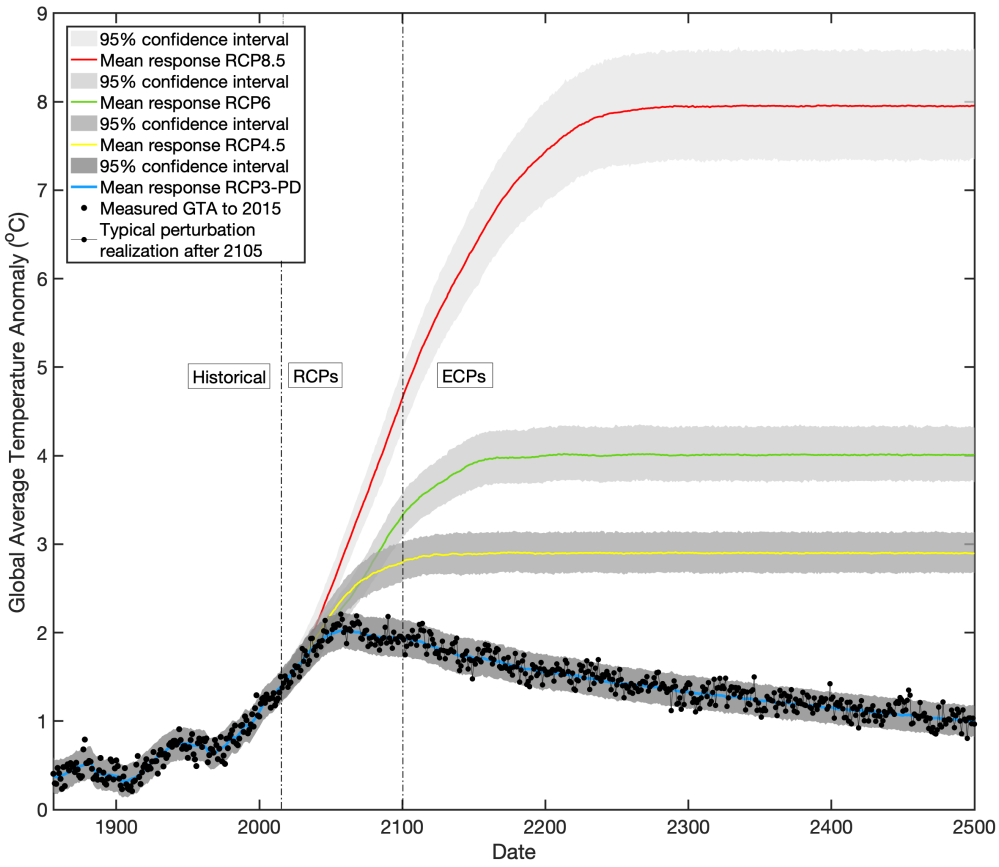

Figure 25: DBM model responses to the four scenarios scenarios in figure 24. *Note that* 95% *confidence bounds are based only on the estimated uncertainty in the model parameters and stochastic perturbations.*

bounds, as in standard short to medium-term forecasting (see Young, 2018).

For example, *and purely for illustration*, figure 26 shows a hypothetical stochastic projection of the DBM model output to 2200, shown as a full red line, based on a forecast of the TRF input similar to that used in Young (2018). The 95% confidence bounds for the full forecast, accounting for the uncertainty in the TRF input forecast as well as the parametric uncertainty in the model, are shown in light grey; while the darker grey bounds are those dependent on the uncertainty in the estimated model parameters alone. From the intersection of the forecast with the red dash-dot line, it can be seen that it reaches a level of 1.5°C above the base GTA level (−0.375°C) at about

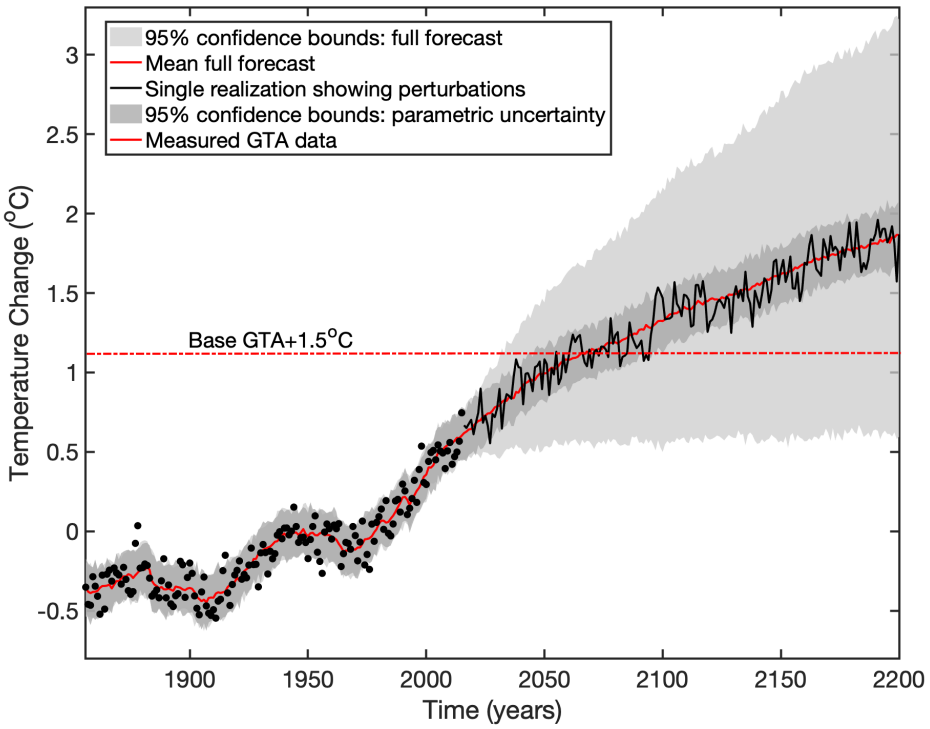

Figure 26: Illustrative hypothetical forecast of the GTA, showing the effects of the uncertainty arising from the parameter estimates, the additive noise and the forecast uncertainty in the TRF input.

2066, or between 2044 and 2094 if the parametric uncertainty is taken into account. Of course, the uncertainty is much greater in the full forecast case. But again, it must be stressed that this example is purely for illustrative purposes.

Finally, note that the different scenarios and the above hypothetical forecast show little effect of the oscillatory state and so have have only a very small effect on the AMO, which is not shown in the plots for this reason. This lack of activity is for two main reasons. First, the future TRF inputs plotted in figure 24 are very smooth, with only minor perturbations, in contrast to the historical series which has significant activity caused by events such as volcanic eruptions. Consequently, the stochastic oscillator is not continually activated and its oscillations are much reduced, as discussed earlier in section 3.2.1 and illustrated in figure 7. Secondly, any such perturbations are

severely attenuated by the averaging process that is an inherent part of MCS analysis.

5 DBM Models and Emission Management

If the DBM models identified and estimated in previous sections are extended to include a model between the emissions input and the atmospheric CO_2 component of the TRF input, then they are in an ideal form for use model-based control system design. The details of a such a study have been presented in a previous Technical Note[11]. Any method of model-based feedback control could be used to design a control system that adjusts the emissions input so that the global temperature follows an acceptable trajectory into the future, so providing guidance about the range and magnitude of the emissions reduction that would be required to control temperature rise, under the assumption that the control model is a reasonable representation of the global temperature dynamics. An exercise of this kind carried out

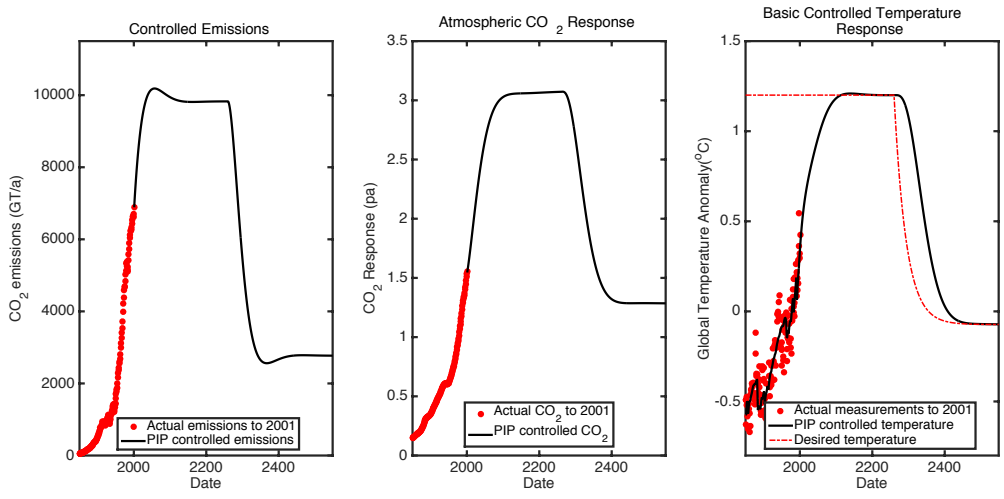

Figure 27: Model-based control of emissions to stabilize CO_2 and global temperature.

some years ago (Young and Jarvis, 2002) using a simpler, less well identified

[11]This report can be downloaded from `http://captaintoolbox.co.uk/Captain_Toolbox.html/Publication_Downloads.html` as `HIDBM_Climate2.pdf`, but note that some of the analysis therein has been superseded by that presented here.

model developed at that time. Subsequently this approach has been used in other studies of a similar nature (Young, 2006; Jarvis et al., 2008). Figure 27 shows the results of a studycarried out using the models identified in Young (2018). We see that the emissions are adjusted so that the global average surface temperature stabilises initially at 1.2^oC and, much later, is reduced to zero, following the 'desired temperature' specification.

6 Conclusions

This report has identified a low dynamic order, stochastic model relating the *Total Radiative Forcing* (TRF) input to the *Globally Averaged Surface Temperature Anomaly* (GTA) and the *Atlantic Multidecadel Oscillation* (AMO). The estimated parameters in this model, together with their estimated covariance matrices, have provided the basis for Monte Carlo simulation analysis that has yielded estimates and 95 percentile uncertainty bounds for the *Climate Sensitivity*, the dominant *Time Constant* (or 'Feedback Response Time') and the *Natural Period* of an oscillatory component that appears to explain the 'climate shifts' discussed in Swanson and Tsonis (2009) and Essex and Tsonis (2018).

This oscillatory component has an estimated period of 55.3 years, with a 95 percentile range between 51.6 and 60 years. Most significantly in climatic terms, the recession periods of this oscillation coincide with and, therefore, are used in the model, to explain the climate shifts ('pauses' or 'levelling') in the generally upward trend of the GTA. Moreover, the period of this oscillatory component is not that different from the 62.5 year period of the AMO and a second order model has been identified between the oscillatory component and the AMO, suggesting a possible link between these two variables.

Clearly, further research is required to establish whether this latter AMO relationship is physically meaningful and what dynamic mechanisms within the complex global climate system might be leading to its influence on the GTA, or vice-versa. Amongst the possible reasons are: the existence of an underlying oscillation in the climate resulting from the interaction of other quasi-cyclical phenomena, such as *Pacific Decadal Oscillation* (PDO), the *North Pacific Index* (NPI), and the *El Nino/Southern Oscillation* (ENSO); or oscillations caused by significant nonlinearities in the system.

The DBM model estimate of the climate sensitivity $\hat{\text{ECS}} = 2.29^oC$, with 95 percentile range of 1.94 to 2.68^oC, is lower and has a smaller range than

that suggested in most climate studies using the large AOGCM models; and it is smaller and more accurate than the $\hat{\text{ECS}} = 2.59^o\text{C}$ estimated as part of the forecasting study in Young (2018). Also the estimated time constant of the GTA response to the TRF of $\hat{T} = 17.5$ years is a little less than the estimate of 19.31 years suggested in the same paper. The smaller values of ECS and T mean that the *theoretical equilibrium level* of the GTA would be reached a little more quickly; or more realistically, that the globally averaged temperature will reach any specified level within a shorter period of time.

As stressed in section 3.1, it is not possible to conduct well planned experiments on the global climate in order to remove the often inherent ambiguity in the observations and so clarify our understanding of the potentially complex mechanisms that underlie the observed behaviour. It is important to realize, therefore, that the analysis and DBM modelling in this report have been applied to a limited data set of 160 annual samples and so any extrapolation of the results any more than a few years into the future must be carried out with great caution, as suggested in section 3.6.

For instance, although the oscillatory component of the identified model is lightly damped and regular in its behaviour, it cannot be assumed that this behaviour will continue like this into the future. It was for this reason that this oscillatory component was considered by Young (2018), within a forecasting context, as a quasi-cycle with a possibly changing period and phase, and was modelled by a *time variable parameter* dynamic harmonic regression model. Furthermore, all of the model response is stimulated by the TRF input, which is dependent on carbon emissions and natural effects, such as volcanic activity, all of which are difficult to predict.

The discerning reader who is relatively new to climate modelling but acquainted with the dynamic behaviour of other natural dynamic systems may well be surprised that the globally averaged climate data can be modelled as a simple, linear dynamic process. As discussed briefly in sections 3.7.3 and 3.8, it is safer to assume that this linear-like behaviour is representing the relatively small perturbations of the climate over the 160 year observational interval and that the underlying system is probably nonlinear. If so, it may well be subject to the more drastic changes that typify the behaviour of nonlinear stochastic dynamic systems.

Finally, it has to be emphasized that a model is only as good as the data on which it is estimated. The data here consist of the three series TRF, GTA and AMO, all of which are based on measured data that has been processed to produce the averaged responses. Most importantly, the TRF

total radiative forcing is a constructed series produced by climate scientists. and so the modelling results presented in this report are dependent upon the efficacy of this TRF series.

7 APPENDICES

A Estimating Initial Condition Effects in RIVC Estimation

The best way to illustrate how initial conditions can be accounted for in RIVC estimation is to consider the first order TF between $u(t)$ and $x(t)$ in the differential equation model (4) in section 3. This defines a differential equation of the form:

$$\frac{dx(t)}{dt} + a_1 x(t) = b_0 \frac{du_1(t)}{dt} + b_1 u_1(t) \tag{37}$$

and the Laplace transform of this model (see e.g. Kuo and Golnaraghi, 2002) yields:

$$sx(s) + x(0) + a_1 x(s) = b_0 s u_1(s) + u_1(0) + b_1 u_1(s) \tag{38}$$

so that,

$$x(s) = \frac{b_0 s + b_1}{s + a_1} u_1(s) + \frac{u_1(0) - x(0)}{s + a_1} 1.0 \tag{39}$$

As a result, it is straightforward to incorporate an allowance for initial condition effects into the RIVC algorithm by adding an additional constant input set to unity over the whole observational interval. The initial conditions are then estimated as the parameter(s) of the second TF in (39) that is associated with this additional input (here, a single parameter defined by $x(0) + u_1(0)$); and the output of this TF adds a response to the output that accounts for the effects of the initial conditions, so ensuring a better explanation of the data over the time it takes for the effects of the initial conditions to decay. This time can be considerable in some cases, so accounting for the initial condition effects can be very important. Finally, note that it may be necessary in practice to increase the order of the numerator in the second TF to fully account for the initial condition effects.

B The Simulink Model

A Simulink diagram of the final DBM model (17) is shown on the next page in figure 28. Here, the blocks containing $\frac{1}{s}$ are integrators that contain the initial conditions on the associate output variables, while the the triangles on their side are the model parameters. The states $x_1(t)$, $x_2(t)$ are denoted by 'ym1' and 'ym2', respectively; and the sum of these, constituting the model estimate of the GTA, is denoted by 'ym'. The lower part of the diagram is the feedback decomposition of the model generating the estimate of the AMO from 'ym2', where the input time delay is 18 years and the parameters are: a=-0.0518; b=-0.1346; c=-0.05595; and d=0.05489 (see sections 3.5 and 3.7.3).

This Simulink model is used in the final model estimation, where the parameters are estimated by prediction error minimization using a customized m-file that expoits the Matlab lsqnonlin optimization routine. In this optimization procedure, the Simulink model is called and run at each step in the optimal search procedure, which also involves the first order discrete-time autoregressive noise model (19). This is not shown in the diagram but it is required to generate the one-year-ahead prediction errors.

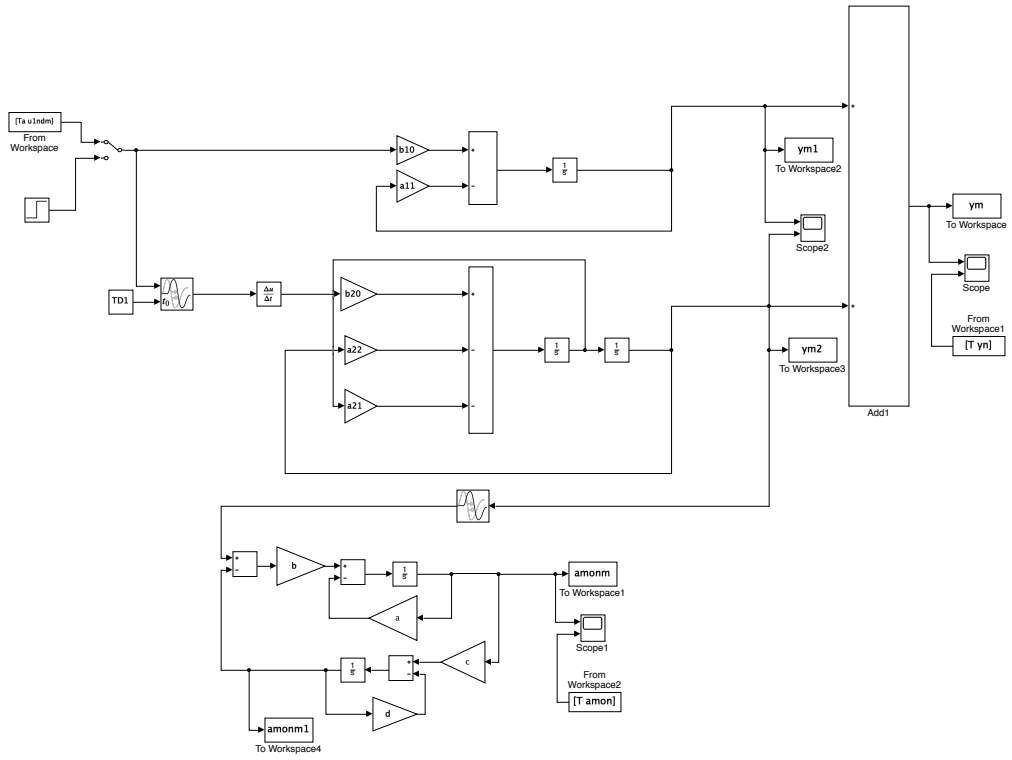

Figure 28: Simulink diagram of the final DBM model (17)/(18) used in the final model estimation.

References

Andrews, D. G. and M. R. Allen (2007). Diagnosis of climate models in terms of transient climate response and feedback response time. *Atmospheric Science Letters 9*, 7–12.

Beer, T. and P. C. Young (1983). Longitudinal dispersion in natural streams. *Am. Soc. of Civil Eng., Jnl. Env. Eng. 109*, 1049–1067.

Beven, K. J. and P. C. Young (1988). An aggregated mixing zone model of solute transport through porous media. *J. Contam. Hydrol. 3*, 129–143.

Box, G. E. P. and G. M. Jenkins (1970). *Time Series Analysis Forecasting and Control*. Holden-Day: San Francisco.

Box, G. E. P., G. M. Jenkins, and G. C. Reinsel (1994). *Time Series Analysis: Forecasting and Control* (3rd ed.). Upper Saddle River, NJ, USA: Prentice Hall PTR.

Chen, F. and P. C. Young (2019). A simple robust method of fractional time delay estimation for linear dynamic systems. *submitted for publication*.

Essex, C. and A. A. Tsonis (2018). Model falsifiability and climate slow modes. *Physica A: Statistical Mechanics and its Applications 502*, 554–562.

Garnier, H. and P. C. Young (2014). The advantages of directly identifying continuous-time transfer function models in practical applications. *Int. J. Control 87*(7), 1319–1338.

Jarvis, A. J., P. C. Young, D. T. Leedal, and A. Chotai (2008). A robust sequential CO_2 emissions strategy based on optimal control of atmospheric CO_2 concentrations. *Climate Change 86*, 357–373.

Kaufmann, R. K., H. Kauppi, and J. H. Stock (2006). Emissions, concentrations and temperature: a time series analysis. *Climate Change 77*, 249–278.

Kuo, B. C. and F. Golnaraghi (2002). *Automatic Control Systems*. New York, NY, USA: John Wiley & Sons, Inc.

Meinshausen, M., S. J. Smith, K. Calvin, J. S. Daniel, M. L. T. Kainuma, J.-F. Lamarque, K. Matsumoto, S. A. Montzka, S. C. B. Raper, K. Riahi, A. Thomson, G. J. M. Velders, and D. P. van Vuuren (2011, Aug). The rcp greenhouse gas concentrations and their extensions from 1765 to 2300. *Climatic Change 109*(1), 213.

Mills, T. C. (2009). How robust is the long-run relationship between temperature and radiative forcing? *Climatic Change 94*, 351–361.

Myhre, G., E. J. Highwood, K. P. Shine, and F. Stordal (1998). New estimates of radiative forcing due to well mixed greenhouse gases. *Geophys Res Lett 25*, 2715–2718.

Price, L., P. C. Young, D. Berckmans, K. Janssens, and J. Taylor (1999). Data-based mechanistic modelling and control of mass and energy transfer in agricultural buildings. *Annual Reviews in Control 23*, 71–82.

Priestley, M. B. (1988). *Nonlinear and Nonstationary Time Series Analysis*. London: Academic Press.

Schlesinger, M. and N. Ramankutty (1994). An oscillation in the global climate system of period 65-70 years. *Nature 367*, 723–726.

Swanson, K. L. and A. A. Tsonis (2009). Has the climate recently shifted? *Geophysical Research Letters 36*, L06711 1–4.

Wallis, S. G., P. C. Young, and K. J. Beven (1989). Experimental investigation of the aggregated dead zone model for longitudinal solute transport in stream channels. *Proc. Inst. of Civil Engrs, Part 2 87*, 1–22.

Young, P. C. (2006). The data-based mechanistic approach to the modelling, forecasting and control of environmental systems. *Annual Reviews in Control 30*, 169–182.

Young, P. C. (2011). *Recursive Estimation and Time-Series Analysis: An Introduction for the Student and Practitioner*. Springer-Verlag, Berlin.

Young, P. C. (2012). Data-based mechanistic modelling: natural philosophy revisited? In L. Wang and H. Garnier (Eds.), *System Identification, Environmetric Modelling and Control*, London, pp. 321–340. Springer-Verlag.

Young, P. C. (2014). Hypothetico-inductive data-based mechanistic modelling, forecasting and control of global temperature. Technical report, Lancaster Environment Centre, Lancaster University, UK.

Young, P. C. (2015). Refined instrumental variable estimation: Maximum likelihood optimization of a unified Box-Jenkins model. *Automatica 52*, 35–46.

Young, P. C. (2016). Data-based mechanistic modeling. In V. P. Singh (Ed.), *Handbook of Applied Hydrology*, Chapter 33, pp. 1–12. USA: McGraw Hill.

Young, P. C. (2018). Data-based mechanistic modelling and forecasting globally averaged surface temperature. *International Journal of Forecasting 34*, 315–334.

Young, P. C. (2019). New results on the DBM modelling, forecasting and control of global climate data.

Young, P. C. and A. J. Jarvis (2002). Data-based mechanistic modelling, the global carbon cycle and global warming. Technical Report TR 177, Centre for Reearch in Environmental Systems (CRES), Lancaster University.

Young, P. C. and M. J. Lees (1993). The active mixing volume: a new concept in modelling environmental systems. In V. Barnett and K. Turkman (Eds.), *Statistics for the Environment*, pp. 3–43. J. Wiley: Chichester.

Young, P. C., M. J. Lees, A. Chotai, W. Tych, and Z. S. Chalabi (1994). Modelling and PIP control of a glasshouse micro-climate. *Control Engineering Practice 2*, 591–604.

Young, P. C., D. J. Pedregal, and W. Tych (1999). Dynamic harmonic regression. *Jnl. of Forecasting 18*, 369–394.

Young, P. C., L. Price, D. Berckmans, and K. Janssens (2000). Recent developments in the modelling of imperfectly mixed airspaces. *Computers and Electronics in Agriculture 26*, 239–254.

Young, P. C. and M. Ratto (2009). A unified approach to environmental systems modeling. *Stochastic Environmental Research and Risk Assessment 23*, 1037–1057.

Young, P. C. and S. G. Wallis (1993). Solute transport and dispersion in channels. In K. J. Beven and M. J. Kirkby (Eds.), *Channel Network Hydrology*, Chichester, pp. 129–173. J. Wiley.